

Review article

Geochronology, geochemistry, and geodynamic evolution of Tatric granites from crystallization to exhumation (Tatra Mountains, Western Carpathians)

ELIZABETH J. CATLOS^{1,✉}, IGOR BROSKA², MILAN KOHÚT², THOMAS M. ETZEL^{1,3}, J. RICHARD KYLE¹, DANIEL F. STOCKLI¹, DANIEL PAUL MIGGINS⁴ and DANIEL CAMPOS¹

¹Department of Geological Sciences, Jackson School of Geosciences, The University of Texas at Austin, Austin, TX 78712, USA;

✉ ejcatlos@jsg.utexas.edu

²Earth Science Institute of the Slovak Academy of Sciences, Dúbravská cesta 9, 840 05 Bratislava, Slovakia

³ExxonMobil, 22777 Springwoods Village Parkway, Spring, TX 77389, USA

⁴College of Earth, Ocean, and Atmospheric Sciences, Oregon State University, 104 CEOAS Admin Bldg. Corvallis, OR 97331-5503, USA

(Manuscript received February 9, 2022; accepted in revised form June 28, 2022; Associate Editor: Rastislav Vojtko)

Abstract: The Western and High Tatra Mountains (northern Slovakia, southern Poland) contain the best-exposed rocks record within the Carpathian orogenic belt. Petrological, geochemical, and geochronological data from granitic assemblages across the Western (n=1) and High Tatra Mountains (n=19) were used to understand how they responded to an extended tectonic and magmatic history. Laser Ablation-Inductively Coupled Plasma-Mass Spectrometry (LA-ICP-MS) zircon dating shows a dominant Early Carboniferous (Tournaisian, TuffZirc age=349.3±2.9/–1.5 Ma at 95 % confidence, n=119 spots), but Paleoproterozoic/Neoproterozoic (2544±33 Ma, ±1σ) to Late Carboniferous (Kasimovian, 305.8±6.2 Ma) dates were also found. The age pattern is consistent with granitic assemblages within the European Variscan belt and suggests an affinity with Armorican terranes derived from a northern Gondwanan Cadomian arc. The final stages of Variscan orogenic collapse are timed at ca. 315 Ma based on the youngest zircon age population. Monazite dated in thin section are also Tournaisian, but the youngest age is Permian (Th–Pb, 270.0±9.1 Ma, ±1σ), consistent with timing of large-scale Pangean Permian extension. High Tatra granite K-feldspar ⁴⁰Ar/³⁹Ar ages indicate slow post-magmatic cooling after granite crystallization. The oldest ⁴⁰Ar/³⁹Ar ages from two samples near Lomnický štít (LS) suggest a thermal event in the Late Triassic (~220 Ma), but others from the sub-Tatra fault and near Gerlachovský štít (GS) are younger (Early Cretaceous, ~120 Ma). The thermal history from K-feldspar at the base of LS shows pulsed exhumation at faster rates between 70–55 Ma (300–200 °C) and 45–35 Ma (200–100 °C). The results document the Paleo-Alpine tectonic imprint of the Western and High Tatra Mountains until the onset of more Neo-Alpine exhumation. The data point to uplift earlier than suggested by models of extrusion tectonics applied to the region. Early uplift is connected with Eocene ALCAPA (ALps–Carpathians–Pannonia) escape leading later to the development of the Carpathian arc.

Keywords: granitoids, geochemistry, Slovakia, zircon, monazite, K-feldspar geochronology, Tatra Mts., Western Carpathians

Introduction

The Carpathians are one of many orocline (curved) mountain belts prominent throughout Europe and are associated with the closure of several ancient oceans and/or relative motion of continental crust fragments which lay between the European and African plate (Fig. 1; Ratschbacher et al. 1991; Royden et al. 1983; Royden & Báldi 1988; Seghedi & Downes 2011). Arcuate orogenic belts are present throughout the globe, and understanding their origin has been a fundamental problem in tectonics, critical for deciphering the nature of plate tectonics and the mechanics of forming plate boundaries (e.g., Carey 1955; van der Voo 2004; Weil et al. 2010). The Carpathians are considered a best example of a curved orogenic belt created by Alpine tectonics. The Western Carpathian Mountains,

in particular, have been a focus of fundamental models for the development of the lithosphere that advanced our understanding of the crustal response to collision. These include extrusion tectonics, orogenic collapse, and subduction rollback (Royden et al. 1983; Ratschbacher et al. 1991; Plašienka et al. 1997; Poller et al. 2001a; Sperner et al. 2002; Kováč et al. 2007; Froitzheim et al. 2008; Plašienka 2018a, and citations therein). Although the evolution of these mountains has been stated to be “critical” to understanding the Cenozoic development of the central parts of the Western Carpathians, little consensus exists regarding underlying controls on its development (e.g., Anczkiewicz et al. 2015; Śmigielski et al. 2016).

The Carpathian Mountains is an amalgamation of crustal fragments juxtaposed due to the closure of ocean basins from the Precambrian to the Miocene (Royden & Báldi 1988; Kováč et

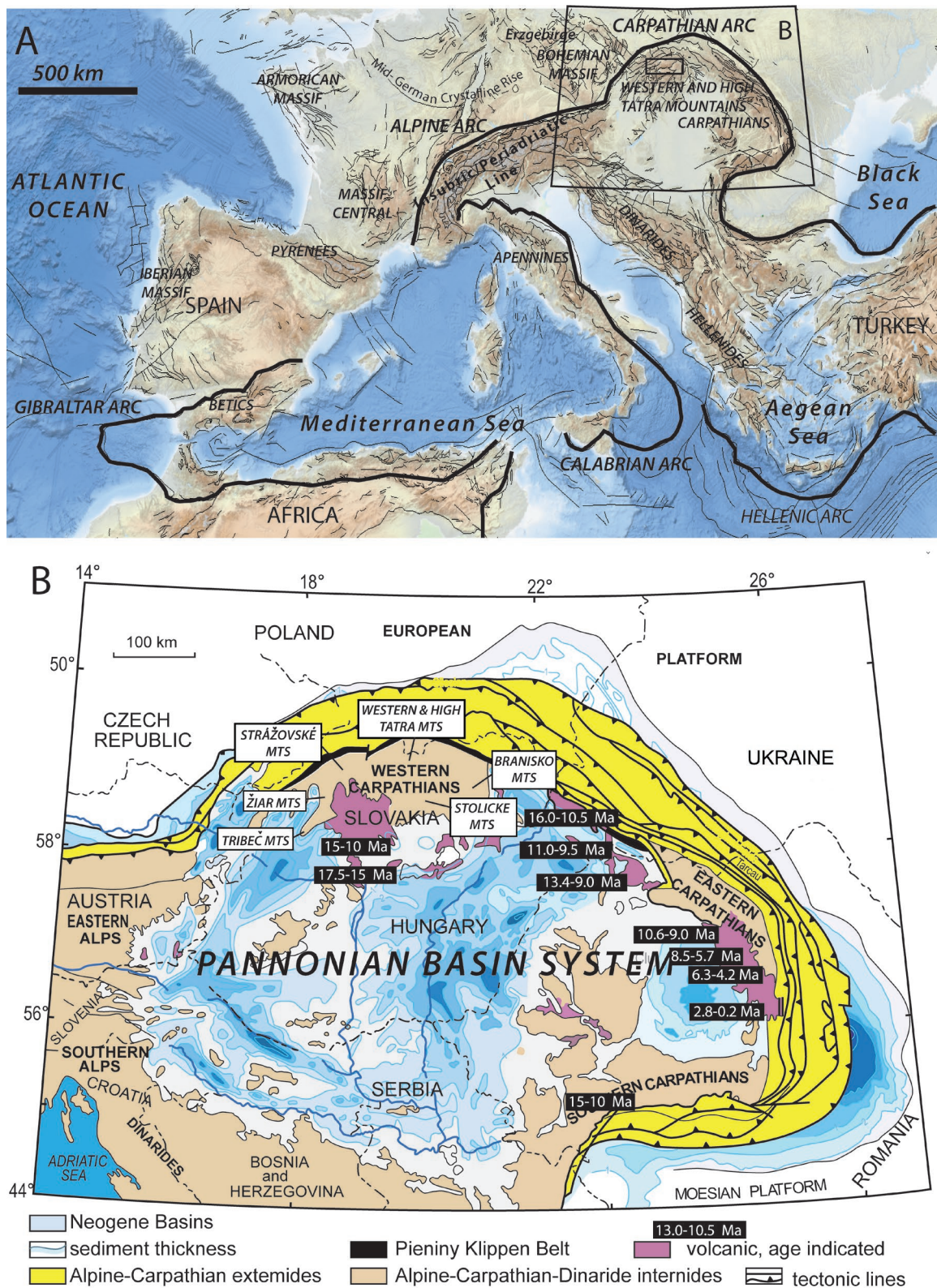


Fig. 1. A — Geological Surveys of Europe (EuroGeoSurvey) map of the Mediterranean area with main curved orogenic systems identified (after Cifelli et al. 2016). Approximate location of the Western and High Tatra Mountains (Fig. 2) is indicated. Faults are from the Europa faults (IGME 5000) and Europe Offshore Faults (IGME 5000) geological map. Data source: IGME5000, © BGR Hannover 2007. Locations of some major massifs and the Mid-German Crystalline Rise after Zeh et al. (2001). **B** — The Alpine–Carpathian–Pannonian–Dinaride domain after Kováč et al. (2007). The approximate location of the Western and High Tatra Mountains are indicated. Ages of volcanic rocks (Ma) indicted as compiled by Hippolyte et al. (1999).

al. 2007; Froitzheim et al. 2008; Kováč et al. 2018, Plašienka 2018a). Consequently, paleogeographic reconstructions of the area have been of interest to those seeking to decipher how the arcuate mountain range formed (Csonotos & Vörös 2004; Schmid et al. 2008). The Western and High Tatra Mountains (Fig. 2), located in northern Slovakia and southern Poland, contain the best-exposed rock record in the Western Carpathians and is a logical target for deciphering its tectonic history (e.g., Anczkiewicz et al. 2015). The basement consists of pre-Mesozoic metamorphic and granitic rocks overlain by sedimentary cover sequences and nappes contouring the crystalline core in the north (Nemčok et al. 1993; Plašienka et al. 1997; Plašienka 2003; Bezák et al. 2011; Anczkiewicz et al. 2015). Metamorphic rocks are more abundant in the Western Tatra Mountains and are only found as xenoliths or lenses in the High Tatra Mountains.

Although Precambrian and Cambrian/Ordovician restitic zircon ages have been reported (Poller & Todt 2000; Kohút et al.

2008; Burda & Klötzli 2011; Gawęda et al. 2016b), the majority of granitic magmatism in the Western and High Tatra Mountains occurred from the Late Devonian to Upper Carboniferous (370–315 Ma) (Burchart 1968; Kohút & Janák 1994; Gawęda 1995; Poller et al. 1999, 2000; Poller & Todt 2000; Burda & Klötzli 2011; Burda et al. 2011, 2013a,b; Broska et al. 2013; Gawęda et al. 2016b, 2019; Broska & Svojtka 2020; Kohút & Larionov 2021; Broska et al. 2022). Here, we report whole-rock geochemical and geochronological data (U–Pb zircon, Th–Pb monazite, and ⁴⁰Ar/³⁹Ar K-feldspar) from twenty granitoid samples collected from the Western (n=1) and High Tatra Mountains (n=19). Some of the zircon, monazite, and K-feldspar ages we obtained have rarely been reported from the region. The pattern of the ⁴⁰Ar/³⁹Ar K-feldspar ages suggests the range experienced slow cooling after crystallization at a time earlier than anticipated based on previous models. Overall, the results are used to outline the earliest tectonic history of the Western and High Tatra

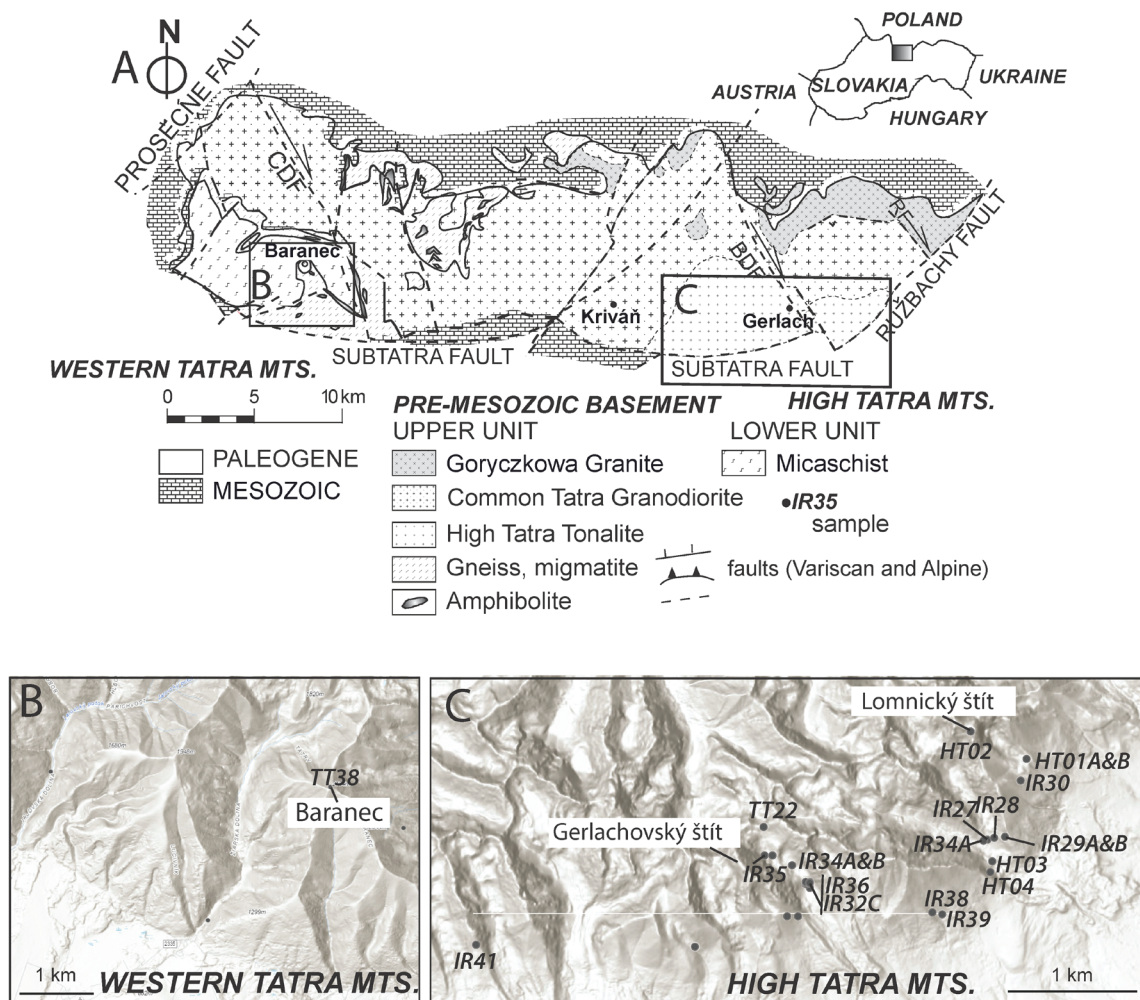


Fig. 2. A — Geologic map of the Western and High Tatra Mountains (Kohút & Janák 1994). Inferred locations and senses of motion for lineaments (CDF=Czarny Dunajec Fault, BDF=Biały Dunajec Fault, RF=Rieka Fault) after Sperner et al. (2002) and Jurewicz (2005). BDF also termed Białka Deep Fault Zone, and RDF is also known as the Rijeka Deep Fault Zone (Wołosiewicz 2018). The Prosečné Fault (after Králíková et al. 2014; Szczygiel 2015) has also been named the Krowlarki Fault (Anczkiewicz et al. 2013) or the Orava Fault (Baumgart-Kotarba et al. 2004). Insets show the sample location maps in panels B and C. See Table 1 for specific locations, assemblages, and rock types.

Table 1: Sample GPS locations and mineral assemblages of granites analyzed in this study.

Sample	Latitude	Longitude	Mineral assemblage
High Tatra samples			
HT01A	49.1889	20.2330	Ser + Pl + Qz + Bt + Ms + Chl + Ep + Zrn + Mnz + Aln + Ap + Kfs + Py + Ilm + FeO + Ttn
HT01B	49.1889	20.2330	Ser + Pl + Qz + Bt + Ms + Chl + FeO + Zrn + Mnz + Aln + Ap
HT02	49.1952	20.2133	Ser + Pl + Qz + Bt + Ms + Amp + FeO + Chl + Zrn + Mnz + Ap + Py + Ttn
HT03	49.1654	20.2210	Ser + Pl + Qz + Bt + Ms + Amp + Chl + Mnz + Py + Ksp + Ttn + Ilm + Aln
HT04	49.1630	20.2203	Ser + Pl + Qz + Bt + Ms + Chl + Amp + Zrn + Mnz + Kfs + FeO + Ilm + Xtm
IR27	49.1705	20.2193	Ser + Pl + Qz + Bt + Ms + Chl
IR28	49.1709	20.2217	Ser + Pl + Qz + Bt + Ms + Amp + Chl
IR29A	49.1712	20.2252	Ser + Pl + Qz + Ms + Chl
IR29B	49.1712	20.2252	Ser + Pl + Qz + Ms + Chl + Ap + opaque
IR30	49.1839	20.2310	Ser + Qz + Pl + Ms + Bt + opaque
IR32C	49.1595	20.1570	Ser + Qz + Amp + Ms + Ep + Fsp
IR34A	49.1701	20.2178	Pl + Qz + Bt + Ms + Chl + opaque
IR34B	49.1645	20.1508	Ser + Pl + Qz + Chl + Amp
IR35	49.1669	20.1414	Ser + Pl + Qz + Ms + Chl + Ap
IR36	49.1607	20.1571	Pl + Qz + Bt + Ms
IR38	49.1538	20.1998	Ser + Pl + Qz + Bt + Ms + Chl + opaque
IR39	49.1535	20.2034	Ser + Pl + Qz + Chl + Bt + Ms + Ap
IR41	49.1464	20.0404	Pl + Fsp + Qz + Bt + Ms + Chl + Amp
TT22	49.1733	20.1408	Ser + Pl + Qz + Fe-rich Chl + Amp + Ap + opaque
Western Tatra sample			
TT38	49.1740	19.7410	Qz + Bt + Pl + Ser + Ms

Mountains until the onset of more recent exhumation and the results are discussed in the context of some other Variscan European granitoids.

Geological background

Variscan and older tectonics

The Western and High Tatra Mountains are located in the Western Carpathians, which extends from the Danube Valley in Austria through Moravia and Slovakia to Poland to the Ukrainian border (Uh River Valley) (Figs. 1 and 2) (Uhlíř 1903; Andrusov 1968; Pícha et al. 2006; Froitzheim et al. 2008; Plašienka 2018a). This portion is bounded to the north by the Western European Platform, which differs from the Eastern Carpathians, which has the Eastern European Platform as its northern boundary. The NW–SE to N–S Eastern Carpathians comprise a part of eastern Slovakia and Poland to Ukraine and eastern Romania (Roca et al. 1995). The Moesian Platform binds the Southern Carpathians. This segment trends E–W, and is primarily located in Romania (e.g., Roca et al. 1995).

The Western Carpathians is divided into inner and outer domains, effectively by the narrow 0.4 to 19 km thick and ~600 km long Pieniny Klippen belt or zone (Andrusov 1968; Ratschbacher et al. 1993; Nemčok & Nemčok 1994; Şengör 2003; Jurewicz 2005; Froitzheim et al. 2008; Chorowicz 2016; Plašienka 2018a, b; Hók et al. 2019). These domains differ in both lithology and timing of deformation (Andrusov 1968; Csontos & Vörös 2004; Schmid et al. 2008; Plašienka 2018a, b). The Inner Western Carpathians are thought to record an older deformation

history in the Late Jurassic to Late Cretaceous (Paleo-Alpine), whereas the Outer Western Carpathians experienced Paleogene to Neogene (Neo-Alpine) thrusting and deformation (Andrusov 1968; Pícha et al. 2006; Froitzheim et al. 2008; Plašienka 2018a, b, 2019). The Outer Western Carpathians has been modelled as a progradational thin-skinned thrust belt (e.g., Pícha et al. 2006; Gaĝala et al. 2012), whereas the Inner Western Carpathians are formed by northward propagating thick-skinned thrust sheets of Variscan basement and Mesozoic cover (e.g., Castelluccio et al. 2015).

The focus of this paper is on the Inner Western Carpathian portion of the Western and High Tatra Mountains. The Western Tatra Mountains is considered a metamorphic envelope complex of the Tara granitic assemblages (Gawęda et al. 2000). The basement of the Western Tatra Mountains is divided by an un-named large-scale Variscan thrust fault that separates Lower Unit mica schists from Upper Unit migmatites and granitoid bodies, creating an inverted metamorphic sequence (Fig. 2) (Kahan 1969; Janák 1994; Janák et al. 1999, 2022; Moussallam et al. 2012). The Lower Unit is composed of ~1000 m thick complex of staurolite, kyanite, and sillimanite-bearing mica schists with local intercalations of quartz-rich metapsammites with a flyschoid character. This unit shows a metamorphic zonation where mineral assemblages in metapelites and P–T conditions record increasing metamorphic grade from 570–640 °C at a pressure (P) of 600–700 MPa. Metamorphic zonation in the Lower Unit is inferred to be a consequence of Variscan overthrusting and emplacement of the Upper Unit, and is locally disturbed by Alpine tectonics.

The Upper Unit is composed of granitic lensoidal intrusions within migmatites and banded amphibolites (mafic and felsic layers alternating on mm to dm scale) with relics of high-P

metamorphism (eclogites with garnet and clinopyroxene, several dm to m scale) occurring at the base of the Upper Unit (Janák 1994; Janák et al. 1996, 2022). Overall this unit is composed of migmatized ortho- and paragneisses, amphibolites, calc-silicates and granitoids, and records two distinct stages of metamorphism, differing in P conditions. An earlier, high-P event M1 reached a temperature (T) of 700–800 °C at 1.0–1.4 GPa, in the kyanite stability field, attaining conditions near the transition between amphibolite–granulite and eclogite facies. It is attributed to subduction (underthrusting) prior to Variscan exhumation. Subsequent low to intermediate P metamorphism M2 in the upper unit reached equilibria in the sillimanite stability field, at 650–750 °C and 400–600 MPa and may be the consequence of recrystallization during decompression and exhumation, closely associated with the emplacement of granitoid pluton penetrating the Upper Unit (Janák 1994; Janák et al. 1999, 2022; Moussallam et al. 2012).

The Upper Unit was intruded by Variscan tongue-shaped granitoids, which are volumetrically dominant in the High Tatra Mountains (Fig. 2). The granitoid rocks are classified into several petrographical types (Kohút & Janák 1994; Burda et al. 2013a, b; Gawęda et al. 2019), attributed to “petrological cannibalism” or mingling and mixing which incremental growth of the pluton occurred over ~30 Myr at 750–850 °C, complicated with different depths of crustal melting (Gawęda et al. 2016b). The types of granitoids include (1) quartz-diorites, (2) biotite granodiorite to tonalites, transitional to muscovite–biotite granodiorites with mafic enclaves and xenoliths of country rocks (High Tatra-type), (3) biotite and muscovite–biotite granodiorites to granites, slightly porphyric (common Tatra-type), (4) granites with K-feldspar and an oriented fabric (Goryczkova-type) (Kohút & Janák 1994; Kohút & Siman 2011). Quartz diorites present in the High Tatra-type are sparsely found within the common Tatra-type in the Western Tatra Mountains. The High Tatra-type is dominant in the central part of the High Tatra Mountains, surrounded (underlying) by the common Tatra-type which is building also a substantial part of the Western Tatra Mountains (Fig. 2). Goryczkova-type granites are found locally at the northern and north-eastern margin of the High Tatra Mountains, with textures that suggest shearing and coarse-grained pegmatitic alteration (Kohút et al. 2009; Kohút & Siman 2011; Burda et al. 2013b). An altered granite sample from the top of Baranec peak in the Western Tatra Mountains (Baranec granite) yields 347±14 Ma zircon age (Poller 2000). Fluorapatite from a coarse-grained felsic dike within a sub-vertical fault zone on Baranec peak are 328.6±2.4 Ma (LA-ICP-MS) (Gawęda et al. 2016a). Zircons from retrogressed eclogite from Baranec Mountain yield 367 Ma and 349 Ma ages, interpreted as growth under eclogite and amphibolite facies metamorphism, respectively (Burda et al. 2021).

The Tatra granitoid pluton is described as a composite polygenetic intrusion (Kohút & Janák 1994) with older (370–360 Ma) apical High Tatra-type granite and local exposures of the Goryczkova type overlying younger Variscan (350–330 Ma) common Tatra-type granites (see discussions in Burchart 1968; Kohút & Janák 1994; Poller & Todt 2000; Poller et al. 2000, 2001a, b; Kohút & Siman 2011; Burda et al. 2013a, b; Gawęda et al. 2016b, 2019; Kohút & Larionov 2021). Interestingly, the quartz diorite

was reported as a younger episode at ~340 Ma (Poller & Todt 2000; Gawęda et al. 2014). Broska et al. (2022) reports zircon ages from a High Tatra diorite xenolith of 359.2±3.0 Ma, and its host granodiorite is slightly younger at 350.1±2.6 Ma.

The evolution of the Tatra Mountains is divided into time frames associated with developing its granitic and metamorphic assemblages and the period associated with exhumation (Fig. 3) (Poller et al. 2000; Janák et al. 2001; Kohút & Sherlock 2003; Jurewicz & Baginski 2005; Králiková et al. 2014; Anczkiewicz et al. 2015; Śmigielski et al. 2016; Burda et al. 2021). Various lithologies have been dated using high- and low-T radiometric approaches to decipher the number and timing of events recorded in the range. The oldest reported zircon ages are Precambrian (3.5–1.8 Ga) and are suggested to be related to precursor migmatites (Janák 1994; Poller & Todt 2000; Kohút & Larionov 2021). Zircons with ~534 Ma cores and ~387 Ma rims are linked to high-grade metamorphism of Eo-Variscan igneous rocks (Burda & Klötzli 2011; Burda et al. 2021). The Cambrian age likely times the consolidation of Cadomian age crust that is linked to the Proto-Carpathian Terrane (530 Ma, 512 Ma; Gawęda et al. 2016b). Ordovician & Silurian zircon ages found from granitic assemblages are linked to melted metasedimentary rocks of Avalonian affinity in a volcanic arc (462 Ma & 426 Ma; Gawęda et al. 2016b).

Early Devonian zircons are suggested to record the onset of granitoid intrusion in the Western Carpathians and partial melting of reworked crustal materials (405 Ma, Poller et al. 2000; 380–370 Ma, Moussallam et al. 2012) or subduction-related magmatism and the formation of the earliest granitoids, precursors of the orthogneisses (406 Ma, Poller et al. 2001a; 385±8 Ma, 368 Ma, Gawęda et al. 2018; 370–368 Ma, Gawęda et al. 2016b; 391±4.6 Ma, Gawęda 2008). The onset of collision is suggested to be 365 Ma with zircon generated in magmatism assemblages from 360–350 Ma (Poller et al. 2000). A biotite tonalite (I-type granite) from the High Tatra Mountains yields a TuffZirc age of 371.5+8.3/–14.0 Ma (n=7, 98.4 % confidence), similar to this time frame (Kohút & Larionov 2021). However, the onset of collision is also timed at 350.1±2.6 Ma based on zircon ages from a High Tatra granodiorite (Broska et al. 2022).

The main magmatic event in the range that produced the voluminous granites occurred during the Lower Carboniferous as recorded by multiple chronometers (Fig. 3) (Poller et al. 2000; Poller & Todt 2000; Poller et al. 2001a, b; Kohút & Sherlock 2003; Burda et al. 2011; Kohút & Siman 2011; Moussallam et al. 2012; Burda et al. 2013a, b; Gawęda et al. 2016b, 2018, 2019). Multiple researchers suggest that significant collisional thickening occurred between 360–340 Ma (Gawęda 1995; Poller et al. 2001a, b; Burda et al. 2013a; Gawęda et al. 2016b, 2019; Kohút & Larionov 2021). The younger limit for Variscan metamorphism linked to granite formation is speculated at 350–340 Ma with emplacement and cooling between 335–305 Ma (Maluski et al. 1993). Poller & Todt (2000) suggest the onset of collision between Laurasia and Gondwana is recorded by High Tatra Mountain diorites at 341±5 Ma, followed by migmatization related to slab detachment of subducted oceanic crust at the active continental margin of Gondwana at 332±5 Ma.

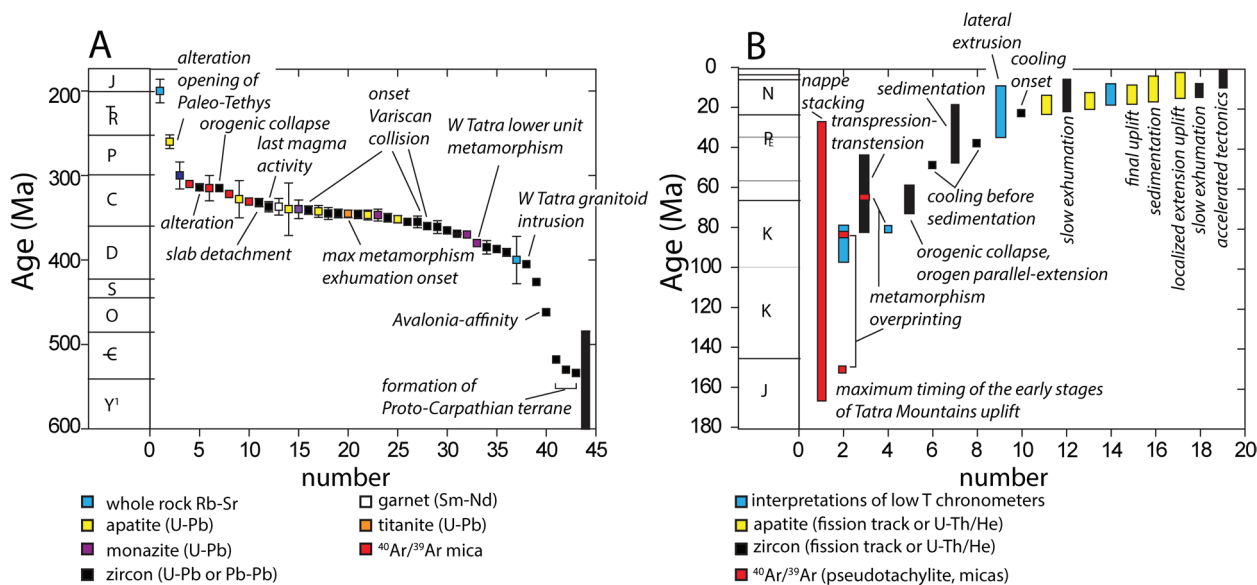


Fig. 3. Summary of reported ages associated with the Western and High Tatra Mountains. The ages are a summary of multiple data points and are considered the “best age” as indicated in the cited references. N=number. Panel (A) shows ages from the Neo-Proterozoic to the Jurassic, whereas panel (B) are Jurassic to present-day. Panel (A) includes majority higher-temperature chronometers, whereas panel (B) are those that time lower temperature events. Data after Burchart (1968); Maluski et al. (1993); Janák (1994); Kováč et al. (1994); Gawęda (1995, 2008); Poller & Todt (2000); Poller et al. (2000, 2001a); Kohút & Sherlock (2003); Kohút & Nabelek (2008); Burda & Klötzli (2011); Moussallam et al. (2012); Anczkiewicz et al. (2013, 2015); Burda et al. (2013a, b); Králiková et al. (2014); Castelluccio et al. (2015); Gawęda et al. (2016b, 2018); Śmigielski et al. (2016); Vozárová et al. (2016, 2019).

Some magmatism extended into the Middle to Upper Carboniferous (328±22 Ma, U–Pb dating of apatite, Gawęda et al. 2018; 300±16 Ma, U–Pb monazite). Burda et al. (2013a, b) suggest that 337±6 Ma records the last magmatic activity followed by younger hydrothermal activity and Pb loss at 314 Ma. Alternatively, the final stages of collision and granite intrusion has been ascribed to 314±4 Ma (Poller & Todt 2000) and orogenic collapse at 315 Ma, based on U–Pb zircon ages (Poller et al. 2001a). Uplift of the basement of the High Tatra Mountains is broadly constrained between 330–300 Ma, based on $^{40}\text{Ar}/^{39}\text{Ar}$ muscovite and biotite ages (Maluski et al. 1993; Janák 1994; Kohút & Sherlock 2003; Moussallam et al. 2012).

Figure 3 highlights challenges in ascribing high and low closure temperature mineral ages to particular events. Zircon and monazite were most often targeted in granitic assemblages to time crystallization. Monazite is more susceptible to dissolution/precipitation reactions due to metamorphism following granite emplacement (e.g., Catlos 2013). Although approaches like LA-ICP-MS generate large volumes of zircon age data, Chemical Abrasion-Isotope Dilution Thermal Ionization Mass Spectrometry (CA-ID-TIMS) appears ideal to remove metamict zones and further refine zircon age precision (Mattinson 2005; Bowring et al. 2006; Gehrels 2012; Catlos et al. 2020). Herriott et al. (2019) compared zircon ages produced by LA-ICP-MS to CA-ID-TIMS and concluded that the LA-ICP-MS Youngest Mode Weighted Mean (YMWM) date best approximates the CA-ID-TIMS date within uncertainty. Tian et al. (2021) also suggest that the YMWM approach is the closest CA-ID-TIMS representation with the requirement of characterizing at least thirty zircon grains for

the youngest mode distribution. Overall, understanding the analytical approach employed to date the Tatra granitoids and their limitations assists in interpreting the results reported here and in Fig. 3.

Alpine-related tectonic history

The Alpine events in geological time control the external morphology of the Tatra Mountains. A dense and regular fault network of mainly strike-slip and extensional structures within the Pannonian Basin system developed the ALCAPA (ALps-CArpathians-PAnnonia) and Tisza Dacia “mega-tectonic units” (e.g., Márton et al. 2007) that propagated into the free lateral boundary of the basin during Neogene (Fig. 4) (Ratschbacher et al. 1991; Hippolyte et al. 1999; Schmid et al. 2008; Lorinczi & Houseman 2010). Deformation was accompanied by a migrating subduction zone of oceanic or thinned continental crust, creating the back-arc nature of the basin (Royden & Horvath 1988, Wortel & Spakman 2000; Márton et al. 2007; Kováč et al. 2016, 2017). Escape of the ALCAPA unit may have begun as early as the Late Eocene (Fodor et al. 1992; Csontos et al. 1992), but “best developed” during the Oligocene (Csontos & Vörös 2004). In the Outer Carpathians, the timing of the last episode of thrusting migrated from west to east from the Late Miocene to Plio-Pleistocene.

Micas from granites in the High Tatra Mountains have been dated using the $^{40}\text{Ar}/^{39}\text{Ar}$ approach, which yields partly disturbed age spectra (Maluski et al. 1991, 1993; Janák & Onstott 1993; Janák 1994; Kohút & Sherlock 2003). Some argon spectra show low-T steps that reveal the younger, Alpine tectonic-thermal over-

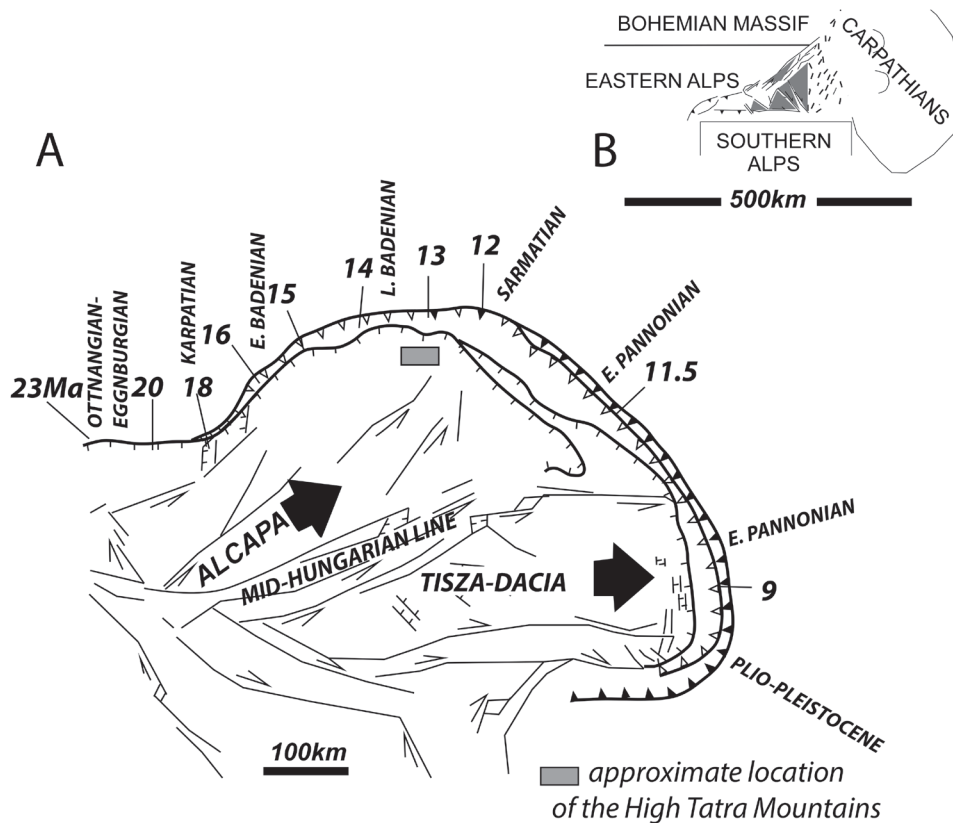


Fig. 4. A — General outline of the Carpathian Mountains with the trend in both age and time frames of the last episode of regional thrusting recorded by sediments in the Outer Carpathians (after Royden & Horvath 1988; Nemčok 1993; Golonka et al. 2006). Map of internal structures and ALCAPA (Alps–Carpathians–Pannonia), and Tisza–Dacia mega-tectonic units after Hippolyte et al. (1999). **B** — Inset shows the indentation experiment extrusion model of Ratschbacher et al. (1991) that appeared to best fit the geology of the Alpine–Carpathian region. A negligible amount of deformation exists to the left of the indenter, as well as asymmetrical faulting and rotated extruded blocks (shaded grey). The Carpathians is illustrated by the rounded shape.

print. The youngest pseudotachylite $^{40}\text{Ar}/^{39}\text{Ar}$ ages ($32\text{--}28\pm 1$ Ma, foothills of Gerlachovský štít) are related to the early stages of uplift of the recent High Tatra Mountains that continued in the Miocene and Quaternary (e.g., Kohút & Sherlock 2003; Jurewicz 2005). Slightly older Eocene (U–Th)/He zircon ages suggest an earlier initiation of the basement unroofing and/or exhumation (Anczkiewicz et al. 2015; Śmigielski et al. 2016). Final uplift is proposed to range between 15 and 10 Ma (Kováč et al. 1994), although fission-track ages have been attributed to accelerated tectonic activity since 10 Ma (Králíková et al. 2014). The last episode of thrusting is regionally speculated to be within the Middle Miocene based on the sedimentary rock record, as thrusting across the Carpathian Arc shifted (Royden et al. 1983; Decker 1996; Schmid et al. 2008).

Methods

We collected samples across the High Tatra Mountains ($n=19$) to generate petrological, geochemical, and geochronological data to understand how they record and responded to an extended tectonic and magmatic history (Table 1; Fig. 2). For comparison, we also collected sample TT38 from the Western Tatra Mountains at

the top of Baranec peak (Baranec granite, Fig. 2). All High Tatra HT#samples, IR27, IR28, IR29A, and IR29B, IR30, IR34A, IR38, and IR39, were taken along a transect towards and near Lomnický štít. Sample HT02 was collected at the peak (Fig. 2C). Samples IR32C, IR34A, IR34B, IR35, IR36, and TT22 are from a transect towards Gerlachovský štít (Fig. 2C). Sample IR41 was collected adjacent to the sub-Tatra Fault (Fig. 2C).

Geochemistry

All rocks were sent to Activation Laboratories in Canada to obtain whole-rock major and trace element compositions. Fusion Inductively Coupled Plasma (ICP) spectrometry was applied to samples using a Perkin–Elmer Sciex Elan 6100 ICP–Mass Spectrometer (MS) to generate all major elements and Sc, Be, V, Ba, Sr, Y, Zr. Fusion ICP–MS was used for all other elements.

Three blanks and five controls (three before and two after) are analyzed per group of samples. Duplicates were fused and analyzed every 15 samples, and the instrument is recalibrated after every 40 analyses. The geochemical data details are provided as supplementary material (Suppl. S1), but Table 2 summarizes some primary geochemical data from the dated igneous assemblages.

Table 2: Summary of geochemical information from dated granitic samples from the High Tatra Mountains.

Analyte symbol ^a	IR27	HT04	HT03	HT02	IR35	IR41	HT01B	HT01A	IR39	IR30
Na ₂ O+K ₂ O (wt%)	6.03	6.31	6.45	7.08	7.19	6.75	6.66	7.47	7.60	6.24
Rock type ^b	GD	GD	GD	GD	G	G–GD	GD	QMGD	GD	GD
Zircon Tsat (°C) ^c	780	763	800	773	782	766	782	773	756	776
Monazite Tsat (°C) ^c	793	781	795	782	810	777	799	759	762	770
Fe/Fe+Mg ^d	0.79	0.80	0.75	0.78	0.757	0.802	0.81	0.82	0.819	0.811
	M	M	M	M	M	M	F–M	F	F	F
MALI ^e	3.22	4.51	4.24	5.56	6.46	4.51	5.21	5.68	5.25	3.31
	C	C	C–A	C–A	C–A	C–A	C–A	CA–AC	C–A	C
ASI ^f	1.10	1.12	1.16	1.17	1.32	1.15	1.28	1.07	1.09	1.10 SP
	SP	SP	SP	SP	SP	SP	SP	P	P	

a. See Fig. 2 for sample locations

b. Abbreviations: QMGD=quartz monzogradiorite, GD=granodiorite, G=granite, G–GD on the boundary between a granite and granodiorite. Summary based on the Na₂O+K₂O (wt%) classification scheme.

c. Zircon saturation temperatures calculated using Watson & Harrison (1983) and monazite saturation temperatures after Rapp & Watson (1986)

d. (FeOtotal)/(FeOtotal+MgO). F=ferroan, M=magnesian granites, based on classification in Frost et al. (2001).

e. MALI=Modified Alkaline Lime Index, C=calcic granite, C–A=calc-alkalic granite, A–C=alkali-calcic granite. CA–AC=on the line between calc-alkalic and alkali-calcic granites.

f. ASI=Aluminosaturation index. SP=strongly peraluminous, P=peraluminous.

Geochronology

Granitoid samples IR27, IR30, IR35, IR39, and IR41 were subjected to common mineral separation techniques to extract zircon grains (150–200 µm in length). All were examined optically during the mounting process to select euhedral grains and eliminate the analysis of cracked or metamict zircons. Zircons were mounted on double-sided tape, and whole grains were dated (n=154 spots) using the Thermo Scientific™ Element2™ High Resolution (HR)Inductively Coupled Plasma-Mass Spectrometry (ICP-MS) with an Excimer (192 nm) laser ablation system instrumentation in the Geo-Thermochronometry lab at the University of Texas at Austin (UT Austin). For Laser Ablation (LA)-ICP-MS analysis, elemental and isotopic fractionation of Pb/U and Pb isotopes, respectively, is corrected by interspersed analysis of primary and secondary zircon standards with a known age [GJ1, n=92, Jackson et al. (2004) and Pak1, n=9, internal age standard; Plešovice, n=9, Sláma et al. (2008)]. All zircon LA-ICP-MS ages discussed in the text are <10 % discordant ²³⁸U–²⁰⁶Pb ages and are reported with ±2σ uncertainty. Zircon grains were also dated in situ (in thin section) using the LA-ICP-MS system in samples HT01A, HT01B, HT02, HT03, and HT04, but most yielded problematic results due to the laser spot size overlapping the matrix. In this case, only the GJ1 (n=27) and Pak1 (n=5) ages standards were used. The supplementary file presents details of the age data (Suppl. S1). Concordia plots and Tables 3 and 4 summarize the results. We also include the Kernel Density Estimation (KDE) plots (Vermeesch 2012) of the same data as a supplementary file (Suppl. S2).

Monazite grains were also dated in the HT samples in situ using the CAMECA ims1270 ion microprobe at the University of California Los Angeles. A 10–15 nA ¹⁶O primary beam focused to a spot 10–15 µm diameter to generate +10 kV secondary ions during this analysis. The mass resolution was set to ~7000, and oxygen flooding was applied to increase Pb+ yields. A 30s presputtering time allowed the removal of potential surficial contamination. Monazite standard 554 was run initially and after every five to six unknown spots. A calibration curve of

ThO+/U+= 0.123(Pb+/U+, Relative SensitivityFactor)+1.309 ±0.092 reproduced the ²³²Th–²⁰⁸Pb age of monazite standard 554 (45±1 Ma, Th–Pb, Harrison et al. 1999) to 46.1±1.5 Ma (±1σ) (n=17, WMA=46.1±0.1 Ma, MSWD=0.4). We also used secondary monazite standard Amelia (Catlos & Miller 2016; 275±1 Ma, ²³⁸U–²⁰⁶Pb ages, CA-ID-TIMS, Peterman et al. 2012), which produced a Th–Pb age of 272.9±11.0 Ma (n=12, WMA=273.3 ±9.2 Ma, MSWD=0.4). The use of the Amelia monazite allowed the generation of U–Pb ages from the monazite grains, which are also reported. In this case, the Amelia monazite was used as a primary age standard as monazite 554 is low in U. Details of both approaches are provided in Supplement S1, and Table 5 summarizes the ages. SIMS data reduction, Concordia diagrams, and age calculations were performed using the software package ZIPS (v3.1.1; Chris Coath, University of Bristol). Common Pb corrections were applied using the evolution model of Stacey & Kramers (1975) and decay constants and ratios recommended by Steiger & Jäger (1977). Uncertainties of the decay constants are included in all U/Th–Pb ages. All SIMS ages are reported with ±1σ uncertainty. KDE plots of the data are included as a supplementary file (Suppl. S2).

K-feldspar in samples IR39, IR27, IR41, and IR35 was also dated using ⁴⁰Ar/³⁹Ar laser geochronology at Oregon State University. K-feldspar separates of 180–250 µm grain size were step-heated using a continuous 25 W Synrad CO₂ laser that incrementally increased from ~0.2 % to 13.0 % total intensity over 29–36 steps. Released gas fractions were analyzed using a Thermo Scientific™ ARGUS VI™ multicollector mass spectrometer. Samples and the Fish Canyon sanidine standard (Kuiper et al. 2008) were irradiated in the Oregon State University TRIGA reactor ICIT facility. Irradiation parameter J for the individual samples was calculated by parabolic interpolation between measure monitors. The estimated uncertainty of this value is between 0.2 % and 0.3 %. K-feldspar from samples HT02 and HT04 were also dated using the ⁴⁰Ar/³⁹Ar approach, but, in this case, the grains were step-heated in a vacuum furnace at Australia National University in 50° increments from 450–1450 °C. Each sample experienced 38 steps in isothermal increments that ranged

Table 3: Summary of LA-ICP-MS ages of zircons extracted from the sample.

Sample (n=) ^a	Oldest age (±1σ, Ma)	% disc. ^b	Youngest age (±1σ, Ma)	% disc. ^c	Average age Carboniferous (±1σ, Ma)	WMA Carboniferous (±1σ, Ma) ^d	MSWD ^e
IR27 (16)	480.0 (14.0)	4.8	333.7 (5.2)	9.5	354.4 (7.1)	344.2 (3.0)	1.0
IR30 (36)	681 (30)	0.9	335.2 (6.2)	0.5	349.8(10.6)	347.0 (2.2)	0.6
IR35 (47)	2544 (33)	3.2	305.8 (6.2)	4.1	345.0 (8.5)	345.4 (1.1)	2.9
IR39 (30)	491 (21)	9.2	312.0 (11.0)	7.1	344.0 (10.1)	343.1 (3.0)	2.4
IR41 (25)	377.4 (9.1)	5.7	327.3 (9.0)	7.3	345.3 (7.0)	343.9 (2.1)	1.9

a. Sample number and number of spots on zircon grains dated from the rock. See Fig. 2 for sample locations.

b. % disc. = percent discordance of the oldest zircon grain dated in the sample.

c. % disc. = percent discordance of the youngest zircon grain dated in the sample.

d. WMA = Weighted Mean Age.

e. MSWD = Mean Square Weighted Deviation of the Weighted Mean Age.

Table 4: Summary of LA-ICP-MS ages of zircons dated in situ (in rock thin section).

Sample name _Grain # ^a	[U] ppm	U/Th	²⁰⁷ Pb/ ²³⁵ U (±2σ)	²⁰⁶ Pb/ ²³⁸ U (±2σ)	RHO ^b	²³⁸ U/ ²⁰⁶ Pb (Ma, ±2σ)	% disc. ^c
HT03_1	472	18.6	0.517 (0.018)	0.066 (0.002)	0.451	410.0 (14.0)	3.1
HT01A_5	223	2.3	0.437 (0.012)	0.060 (0.001)	0.372	372.7 (7.6)	1.0
HT03_2	1281	11.2	0.421 (0.013)	0.057 (0.002)	0.549	358.0 (13.0)	0.5
HT01B_1	108	1.0	0.414 (0.016)	0.053 (0.002)	0.301	335.0 (9.2)	4.6
HT01B_4	567	2.4	0.437 (0.021)	0.053 (0.002)	0.596	335.0 (13.0)	8.7
HT03_6	438	2.3	0.423 (0.028)	0.053 (0.002)	0.677	334.0 (17.0)	6.7

a. Nomenclature is sample name _grain dated.

b. RHO = correlation coefficient.

c. % disc. = percent discordance of the zircon grain dated in the sample.

in duration from 15–70 minutes. All experiment data, including step size heating schedules, are included in the supplementary materials (Excel files S3, S4, S5, S6 and summary file S7). Age calculations for the lased data were handled using ArArCALC v.25.2 (Koppers 2002), whereas those from the step-heated analyses used the MacArgon program (Lister & Baldwin 1996). Table 6 summarizes the numerical results.

Results

Geochemistry

Figure 5A displays the geochemical data for all samples on a Na₂O+K₂O vs. SiO₂ plot (Middlemost 1994). Most of the igneous rocks collected have granodiorite compositions consistent with the common Tatra type, although some are also granite (IR32C, IR35, HT04, IR36), diorite (IR34B), or quartz monzogranodiorite (HT01A). Sample IR36 has the highest SiO₂ contents from all of the analyzed rocks (78.6 wt% SiO₂) (Fig. 5A). The Baranec sample collected from the Western Tatra Mountains (TT38) is a quartz monzonite.

Table 2 summarizes the geochemical data from the rocks dated in this study using the zircon saturation T according to Watson & Harrison (1983) and monazite saturation T after Rapp & Watson (1986), and the Frost et al. (2001) granite classification. In this scheme, most are granodiorites, except IR35 (granite) and HT01A (monzogranodiorite). All studied granitic samples are magnesian, except samples HT01A, IR39, and IR30, which are ferroan according to Frost et al. (2001). Sample HT01B is on the line

between magnesian and ferroan. Most are calcalkalic, except IR27, HT04, and IR30, which are calcic. Sample HT01A is on the line between calc-alkalic and alkali-calcic. All are strongly peraluminous, except HT01A and IR39, which are peraluminous.

Using the trace elements Y+Nb vs. Rb (ppm) (Fig. 5B; Pearce et al. 1984), most rocks fall within the volcanic arc field, except the Baranec quartz monzonite TT38 and High Tatra

Mountains granite IR36. These samples have higher Y contents compared to the other samples (54 ppm, IR36 and 56 ppm TT38). Using a Fe₂O₃/MgO (wt%) vs. Zr+Ce+Y+Nb (ppm) plot (Whalen et al. 1987), all granitoids from the High Tatra Mountains appear to be fractionated felsic granites, except sample IR28, which falls within the A-type region along with Baranec quartz monzonite sample TT38 (Fig. 5C). Using the discrimination diagram of Zhang et al. (2006) (Fig. 5D), most samples cluster in the field of high Sr and low Yb contents, suggesting derivation from high-P sources in equilibrium with eclogitic-facies residues. Exceptions are samples IR35 (field II, magmas derived from moderate-P sources in equilibrium with granulitefacies residues), IR34B (field III, magmas from low-P sources in equilibrium with amphibolitefacies residues), IR36 (field IV, magmas from very low-P sources in equilibrium with gabbroic residues). The Baranec quartz monzonite sample TT38 lies along the line of fields III and IV. According to the Rb/Sr vs. Rb/Ba and CaO/Na₂O vs. Al₂O₃/TiO₂ plots (Sylvester 1998) (Fig. 5E and F), all magmas derive from a clay-poor source indicating a mixture of greywacke with metabasalt. The samples are within the quadrilateral of strongly peraluminous granites, typical of Variscan (Hercynian) granite field (Sylvester 1998).

Table 5: Summary of U–Th/Pb monazite SIMS ages dated in situ.

Grain number, spot ^a	²³² Th– ²⁰⁸ Pb age (Ma, ±1σ)	% ²⁰⁸ Pb ^{+b}	²³⁸ U– ²⁰⁶ Pb age (Ma, ±1σ)	% ²⁰⁶ Pb ^{+c}
HT01A				
m2	346.9 (12.9)	93.89 (0.22)	338.1 (21.9)	82.83 (0.47)
m3	303.8 (10.2)	79.08 (1.26)	220.6 (25.2)	24.19 (2.16)
HT01B				
m1	370.2 (15.5)	98.95 (0.04)	390.2 (31.5)	96.05 (0.16)
m5	325.4 (10.3)	99.75 (0.03)	310.6 (19.5)	95.62 (0.43)
m2	330.0 (26.9)	88.28 (0.40)	267.9 (27.5)	95.17 (0.20)
m6	325.0 (10.6)	96.05 (0.08)	300.9 (16.9)	75.36 (0.52)
HT02				
m1	374.5 (12.2)	99.01 (0.05)	428.6 (27.3)	95.83 (0.30)
m4	366.3 (19.4)	99.64 (0.06)	367.0 (38.5)	98.21 (0.29)
m5	296.8 (26.7)	90.60 (0.46)	191.0 (11.5)	66.41 (1.33)
m6	288.2 (26.5)	73.99 (1.15)	37.6 (20.7)	8.02 (4.36)
HT03				
m3	381.5 (16.3)	98.22 (0.93)	490.9 (52.2)	95.42 (0.22)
m5s1	376.1 (30.0)	99.90 (0.02)	347.9 (44.8)	99.52 (0.09)
m1s1	358.5 (12.3)	99.73 (0.02)	416.5 (29.8)	99.20 (0.05)
m1s2	319.5 (8.0)	99.89 (0.01)	375.0 (23.4)	98.72 (0.12)
m7	310.3 (12.2)	99.68 (0.03)	342.0 (24.6)	97.28 (0.24)
m2	300.4 (9.5)	99.14 (0.04)	141.7 (8.4)	92.49 (0.31)
m8	270.0 (9.1)	99.31 (0.09)	291.3 (20.4)	95.15 (0.61)
HT04				
m4	342.5 (9.9)	96.65 (0.10)	345.1 (13.3)	97.12 (0.12)
m5s1	337.1 (11.3)	99.15 (0.05)	225.9 (7.1)	95.36 (0.28)
m6	329.7 (9.6)	99.23 (0.05)	315.3 (20.8)	93.93 (0.36)
m5s2	318.9 (11.0)	95.02 (0.30)	303.8 (15.7)	85.18 (0.90)

a. Nomenclature is monazite (m) number_spot number.

b. % radiogenic ²⁰⁸Pb.

c. % radiogenic ²⁰⁶Pb.

Using the Heilimo et al. (2010) Ternary discrimination diagram, (Ba+Sr)/1000 represents enriched mantle, Er is related to the non-garnet controlled source and 1/Er indicates a source controlled by garnet. Most High Tatra Mountains samples fall within the enriched mantle source field, except sample IR36 and Baranec quartz monzonite TT38 (Fig. 6A). These samples lie within the non-garnet-controlled source field. Using the Ca+Al–3Al+2(Na+K)–Al+(Na+K) projection diagram that differentiates among the sources and the tectonic setting trends (Moyen et al. 2017; Moyen & Laurent 2018) (Fig. 6B), all samples appear to have a felsic source and lie within the collision-related trend. The data form a linear trend in this diagram from sample IR35 to IR34B. The trend is controlled by the stoichiometry of minerals in the granitoids that contain Ca, Al, Na, and K, but shows a clear mixing line between the mafic and felsic sources.

All studied samples appear to be moderately evolved using their K/Rb vs. SiO₂ contents, except sample IR39, which is unevolved, and sample IR36, which is strongly evolved (Fig. 6C). The rocks appear to have been emplaced primarily at low P (<5 kbar) according to their calcium and aluminum contents using the criteria of Patiño Douce (1999) (Fig. 6D). High Tatra Mountains samples HT04, IR36, and Baranec quartz monzonite TT38 fall outside the low P trendline. Regarding gauging the extent of

Table 6: Summary of ⁴⁰Ar/³⁹Ar age data.

Sample	Oldest step age (Ma) (Ma, ±2σ) (<95 % ³⁹ Ar _k released)	Youngest step age (Ma, ±2σ) (>2 % ³⁹ Ar _k released)	Total Fusion Age (Ma, ±2σ)
IR39	228.81 (0.31)	47.54 (0.10)	184.57 (4.07)
IR27	234.52 (0.31)	38.48 (0.15)	177.38 (3.92)
IR41	143.36 (0.18)	44.10 (0.08)	111.44 (2.48)
IR35	136.47 (0.27)	35.75 (0.11)	135.52 (2.94)
HT02	110.76 (0.79)	57.07 (0.78)	78.73 (0.99)
HT04	90.94 (0.69)	17.01 (2.92)	69.04 (0.92)

their fluid interactions, the rocks have relatively uniform chondrite-normalized Hf/Sm ratios, except sample IR34B and IR36, which suggest subduction fluid-related interaction (Fig. 6E). Samples IR39 and IR32C show more fluid components in their petrogenesis using the Ba/Rb vs. Th/Rb plot (Fig. 6F).

All samples analyzed in this study are LREE enriched and have similar behavior with the elements in the commonly-used spider diagram, with some notable exceptions (Fig. 7). Baranec quartz monzonite sample TT38 and High Tatra Mountains sample IR36 show more significant HREE contents than the other analyses (Fig. 7B and D). Most granitoids have no to slight Eu anomalies, except IR28, which has a positive Eu anomaly (Fig. 7B). This sample is also interesting because it has higher Sr and Sb contents than the other rocks, which is unusual compared to the other

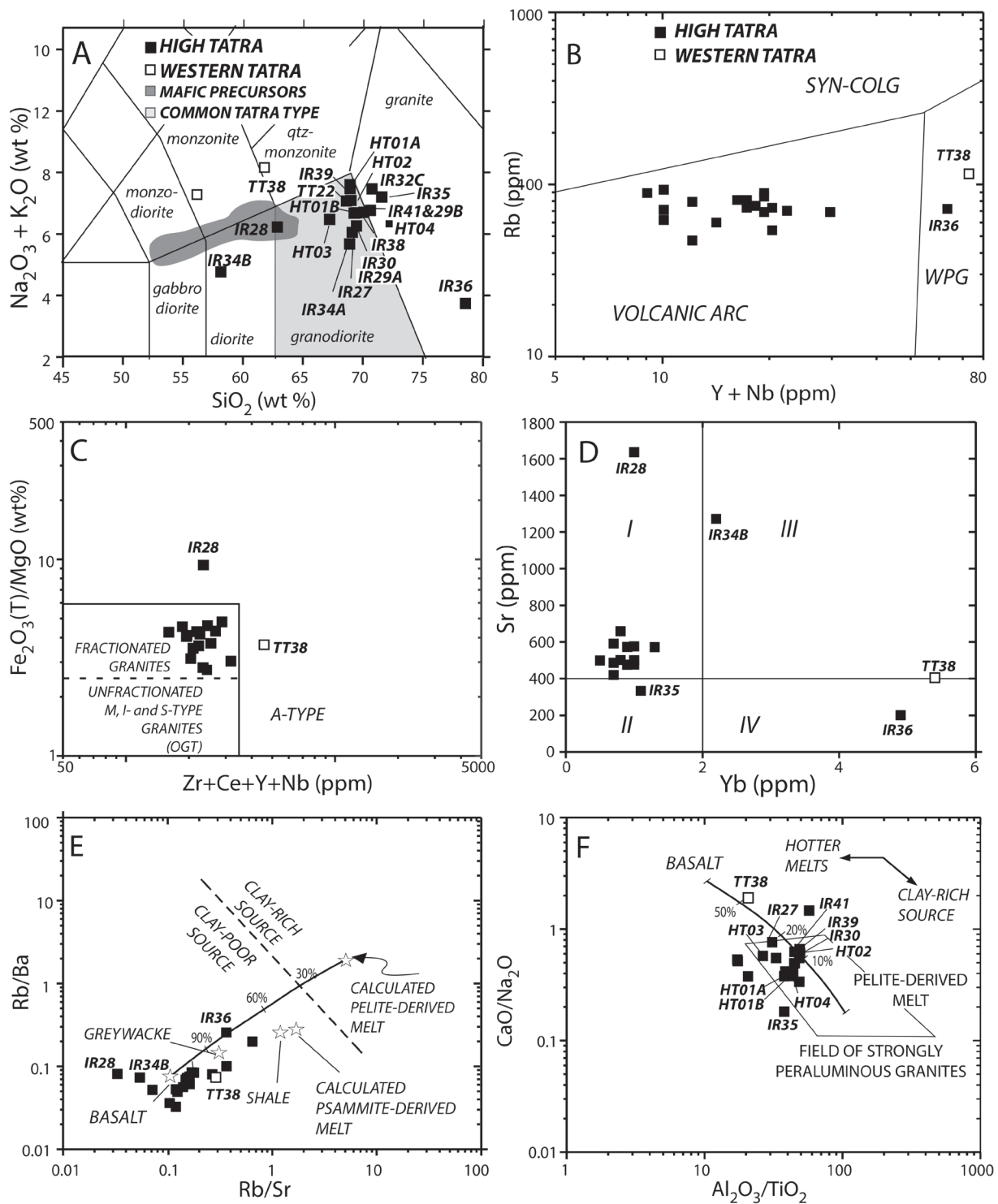


Fig. 5. A — $\text{Na}_2\text{O} + \text{K}_2\text{O}$ versus SiO_2 (wt %) diagram (Wilson 1989) for all samples analyzed in this study. Samples are identified. B — $\text{Y} + \text{Nb}$ (ppm) vs. Rb (ppm) discrimination diagram (Pearce et al. 1984) for the igneous assemblages only. C — Plot of $\text{Zr} + \text{Ce} + \text{Y} + \text{Nb}$ vs $(\text{Fe}_2\text{O}_3(\text{T})/\text{MgO})$ (wt %) showing fields of A-type, fractionated felsic granites, and un fractionated M, I- and S-type granites (OGT, orogenic granite types) after Whalen et al. (1987). D — Yb vs. Sr diagram showing fields (I: magmas derived from high-pressure sources in equilibrium with eclogite-facies residues, II: magmas derived from moderate-pressure sources in equilibrium with granulite-facies residues, III: magmas from low-pressure sources in equilibrium with amphibolite-facies residues, and IV: magmas from very low-pressure sources in equilibrium with gabbroic residues) after Zhang et al. (2006). E — Rb/Sr vs. Rb/Ba diagram after Sylvester (1998). Dashed line divides clay-rich and clay-poor sources. Stars indicates the location of rock-derived melt as labeled. F — $\text{Al}_2\text{O}_3/\text{TiO}_2$ vs. $\text{CaO}/\text{Na}_2\text{O}$ diagram after Sylvester (1998). Quadrilateral designates regions where strongly peraluminous melts from other regions have plotted. In panels (E) and (F), we include a mixing curve between average Phanerozoic basalt and pelite-derived melt (see Sylvester 1998). Percentages of basalt mixing are indicated.

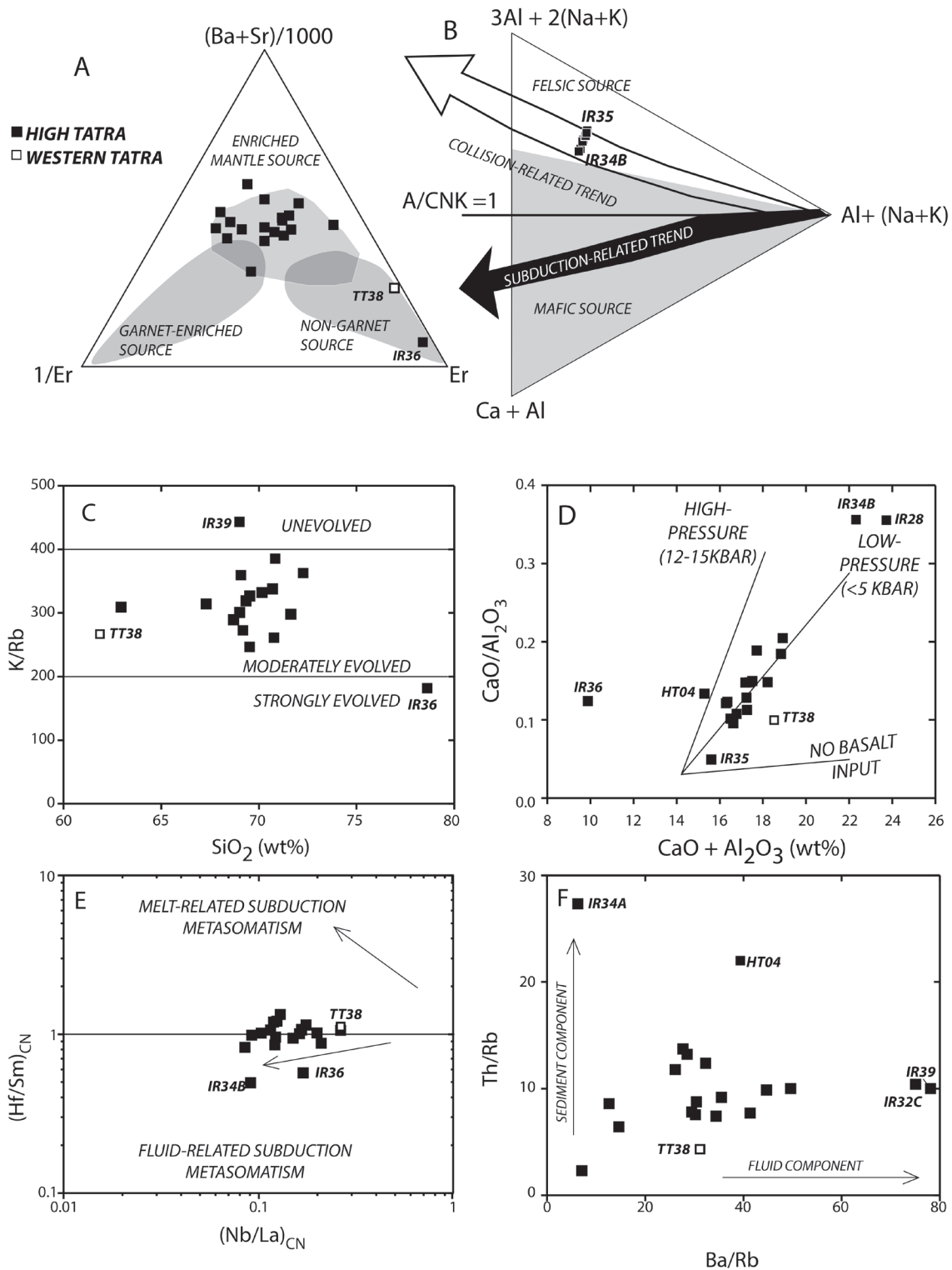


Fig. 6. **A** — Ternary diagram of $Ba+Sr/1000$, $1/Er$ and Er that differentiates between enriched mantle, garnet-controlled and non-garnet-controlled sources (Heilimo et al. 2010). **B** — The $Ca+Al-3Al+2(Na+K)-Al+(Na+K)$ projection diagram that differentiates among the sources and the tectonic setting trends (Moyen et al. 2017; Moyen & Laurent 2018). Plot of Th/Yb vs. Ba/La that allows for the identification of the role of the sediment and fluid components (Woodhead et al. 2001). **C** — Plot of K/Rb vs. SiO_2 that evaluates the evolution of the granites (Blevin 2004). **D** — $CaO+Al_2O_3$ vs. CaO/Al_2O_3 diagram for the analyses after Patiño Douce (1999). Lines indicate trends where high-pressure, low-pressure, and magmas with no basalt input would be located. **E** — Plot of $(Hf/Sm)_{CN}$ vs. $(Nb/La)_{CN}$ chondrite-normalized plot (La Flèche et al. 1998), which allows for the differentiation of the potential metasomatic agent involved in the petrogenesis of Western and High Tatra granites. **F** — Plot of Th/Rb vs. Ba/Rb that evaluates the degree of interaction of the magma with sediment and fluid components (after Woodhead et al. 2001).

samples (Fig. 7D and E). High Sb related to hydrothermal alteration has been found in Western Tatra granites in the Polish portion of the range (Sitarz et al. 2021). Sample IR35 also shows a Ho anomaly (Fig. 7B and D). The Ho anomaly may be related to aqueous interaction in the final stages of crystallization driving a tetrad effect, also observed in highly evolved Variscan (late Hercynian) granites of Germany (Hecht et al. 1999; Irber 1999). We include a supplementary figure showing the relationship of the tetrad effect to various trace element ratios (Y/Ho, Zr/Hf, Eu/Eu*, and Sr/Eu, [Suppl. S8](#)), although the relationship of the tetrad effect to magmatic differentiation and alteration processes is debated (McLennan 1994).

For the dated granitoids (Table 2), the zircon and monazite saturation T overlap and average 775 ± 12 °C and 783 ± 17 °C, respectively. Sample HT03 has the highest zircon saturation T (800 °C), and IR39 has the lowest (756 °C). Samples IR36 and TT38, which were not dated, but compositionally analyzed and show a within-plate granite signature (Fig. 5B) and higher HREE patterns (Fig. 7B), and have zircon saturation T that is on the higher end (787 °C and 768 °C, respectively). Dated sample IR35 has a high monazite saturation T (810 °C), and HT01A has the lowest (759 °C). Samples TT38 and IR36 have higher monazite saturation T than the dated samples, at 840 °C and 818 °C, respectively.

Geochronology

Tables 3 and 4 summarize the concordant U–Pb LA-ICP-MS ages from samples IR27, IR30, IR35, IR39, IR41, and all HT# samples. We report the ages that are only <10 % discordant and show the Concordia diagrams for all samples in Fig. 8. Different statistical approaches can be applied to extract the most robust and accurate ages from LA-ICP-MS ages of a population of dated zircons (e.g., Vermeesch 2012; Coutts, et al. 2019; Herriott et al. 2019; Tian et al. 2021), including TuffZirc (Ludwig & Mundil 2002; Coutts et al. 2019). Table 3 reports the oldest and youngest zircon age, average and weighted mean Carboniferous ages and Mean Square Weighted Deviation of the weighted mean age for the zircons extracted from the samples and dated using LA-ICP-MS. Figure 9 shows the TuffZirc age for all samples and the probability density diagram (PDD) (Ludwig 2003) for the dated zircons and monazites, highlighting the age of each peak. We include the KDE plots (Vermeesch 2012) of the same data as a supplementary file ([Suppl. S2](#)). The KDE analyses have fewer peaks compared to the PDD and results from the KDE analysis are shown in Figs. 8 and 9. The age of the largest peak using the KDE approach overlaps, but is more certain than those estimated using the TuffZirc algorithm (Fig. 9). The following paragraph discusses individual zircon spot data organized by oldest to youngest age.

The oldest grain dated in the study is Paleoproterozoic/Neoproterozoic and is found in the core of a zircon in sample IR35 (2544 ± 33 Ma, 3.2 % discordant). This zircon has a Tournaisian (Early Carboniferous rim, 343 ± 11 Ma, 3.4 % discordant). We also found two Late Neoproterozoic zircons in sample IR30 (681 ± 30 Ma, 8.8 % discordant) and sample IR35 (660 ± 17 Ma,

5.8 % discordant). These zircons have younger rims (Tournaisian, 352 ± 9 Ma, 0.8 % discordant and Devonian, 364 ± 10 Ma, 3.4 % discordant). Two Cambrian zircons were also found in samples IR30 and IR35 (523 ± 29 Ma, IR30; 532 ± 13 Ma, IR35), and two Late Cambrian zircons were dated in sample IR39 (491 ± 21 Ma and 486 ± 12 Ma). Both the oldest and youngest Late Cambrian zircons have Tournaisian rims (353 ± 8 Ma, 3.8 % discordant and 356 ± 9 Ma rim age, 0 % discordant, respectively), as does the zircon with the 532 ± 13 Ma core (352 ± 8 Ma, 0.3 % discordant).

Six Ordovician zircons were found in samples IR30, IR27, and IR41 (from 486 ± 9 Ma to 457 ± 8 Ma), and one grain at the Ordovician–Silurian boundary was dated in sample IR41 (443 ± 17 Ma). Two of the Early Ordovician (486 ± 9 Ma, 473 ± 13 Ma) and one Middle Ordovician zircon (461 ± 26 Ma) have Tournaisian rims (356 ± 9 Ma, 351 ± 9 Ma, and 349 ± 11 Ma, respectively). Thirty-two Devonian zircons were dated in the samples and range from 410 ± 14 Ma (HT03) to 359 ± 6 Ma (IR41). These grains average 370.5 ± 10.2 Ma [weighted mean age, WMA, 367.8 ± 2.2 Ma, Mean Square Weighted Deviation (MSWD) of 1.4].

The majority of zircons dated are Carboniferous ($n=119$ ages), with the majority of these being Tournaisian ($n=112$). Only seven zircons fell into the Late Carboniferous age category (from 328 ± 16 Ma, IR41 to 306 ± 6 Ma, IR35). The average of all Tournaisian ages is 337.6 ± 8.1 Ma (WMA 337.2 ± 1.1 Ma, MSWD= 2.7). The TuffZirc age (Ludwig & Mundil 2002) is also Tournaisian at $349.3\pm 2.9/-1.5$ Ma at 95 % confidence from a coherent group of 119 spots. Using the KDE approach (Vermeesch 2012), the tallest peak is older at 357.4 ± 0.3 Ma (see [Supplement S2](#)). The PDD for all zircons dated using LA-ICP-MS shows the highest peak at 348.4 Ma and a minor younger peak at 315.9 Ma (Fig. 9A). We also identify five additional subtle older age peaks since the Cryogenian.

The zircon grains dated in situ are similar to those we dated using the laser-based approach and are Late Devonian to Carboniferous (410 ± 14 Ma to 334 ± 17 Ma, both grains in sample HT03). Figures 10 and 11 show the BSE images of the dated grains. Zircons range in size from larger, sub to euhedral grains to tiny cubic grains at the edges of biotite. The relationship of zircon and biotite is a common texture in granitic assemblages and is potentially indicative of crystal settling (Ward et al. 1992; Bea 1996; Catlos et al. 2012). The oldest age is within the core of a zircon grain with a younger rim (358 ± 13 Ma) (Fig. 10A).

Monazite was also dated in situ in the same assemblages and range in age from 382 ± 16 Ma to 270 ± 9 Ma (Th–Pb ages, found in sample HT03). The TuffZirc age approach was also applied to all monazite spots (Ludwig & Mundil 2002), which yields $337.8\pm 13.6/-14.7$ Ma at 95 % confidence from a coherent group of 17 spots. The PDD identifies the tallest peak at 332.7 Ma, with a shoulder at 310.3 Ma (Fig. 9B). Most monazite grains in these samples appear in reaction textures. For example, the oldest monazite grain dated is in sample HT03 and is located on the edge of a titanite grain that shows FeO exsolution textures (Fig. 11A). Tiny cubic zircons appear on the edges of the titanite but could not be dated due to their small size. Larger monazite grains are in contact with titanite in this sample

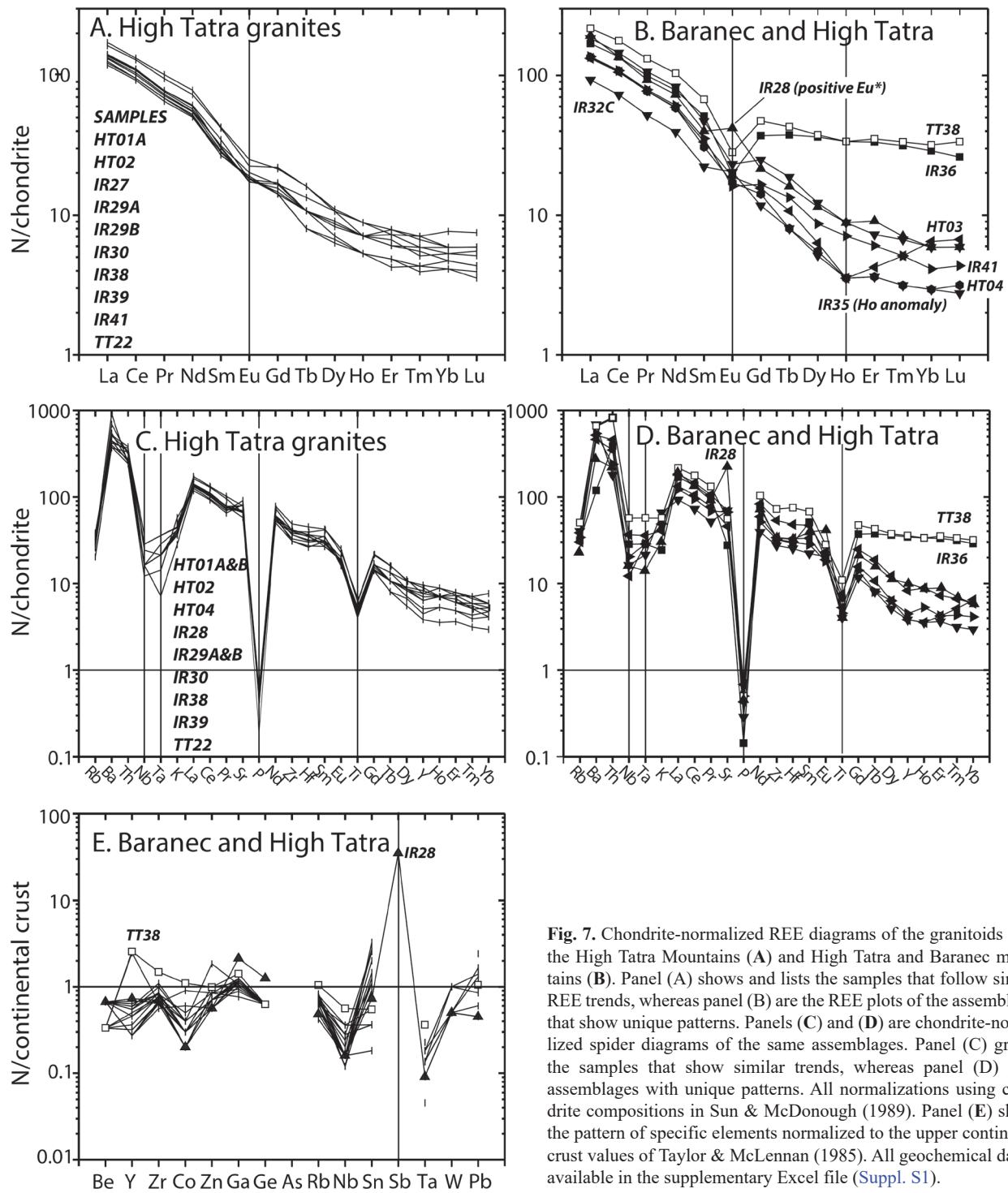


Fig. 7. Chondrite-normalized REE diagrams of the granitoids from the High Tatra Mountains (A) and High Tatra and Baranec mountains (B). Panel (A) shows and lists the samples that follow similar REE trends, whereas panel (B) are the REE plots of the assemblages that show unique patterns. Panels (C) and (D) are chondrite-normalized spider diagrams of the same assemblages. Panel (C) groups the samples that show similar trends, whereas panel (D) plots assemblages with unique patterns. All normalizations using chondrite compositions in Sun & McDonough (1989). Panel (E) shows the pattern of specific elements normalized to the upper continental crust values of Taylor & McLennan (1985). All geochemical data is available in the supplementary Excel file (Suppl. S1).

(Figs. 10A, 11D). Although most monazite grains dated are smaller, anhedral spherical grains, the youngest are in reaction textures with allanite or epidote (Fig. 11K, L, and M). The youngest monazite is Permian (270 ± 9 Ma) and is found in sample HT03 within plagioclase. The PDD of the monazite ages has a distinct peak at 275.5 Ma with a shoulder at 254.5 Ma (Fig. 9B).

We obtained K-feldspar ages from samples IR39, IR27, IR41, and IR35 using laser stepheating (Fig. 12A), whereas sample HT02 and HT04 were step-heated in a furnace (Fig. 12B and C). The lased feldspars and sample HT04 yield age spectra consistent with slow cooling, but the age spectrum from sample HT02 is consistent with the incorporation of excess argon (Fig. 12B). Samples IR39 and IR27 have similar ages from the later degassed

steps of ~220 Ma (Late Triassic), whereas samples IR35 and IR41 have similar but younger ages of ~120 Ma (Early Cretaceous). The youngest $^{40}\text{Ar}/^{39}\text{Ar}$ K-feldspar ages from all lased samples obtained in the early steps average 40.8 ± 0.3 Ma. Sample HT04 yielded an age spectrum similar in shape to those in samples IR35

and IR41 (Fig. 12C). The sample yields only three steps that create a plateau at 81 ± 1 Ma (MSWD 15.6). We applied Multi-Diffusion Domain (MDD) modeling (Lovera et al. 1989, 1991; Harrison & Lovera 2013) to this sample, yielding the thermal history seen in Fig. 12D.

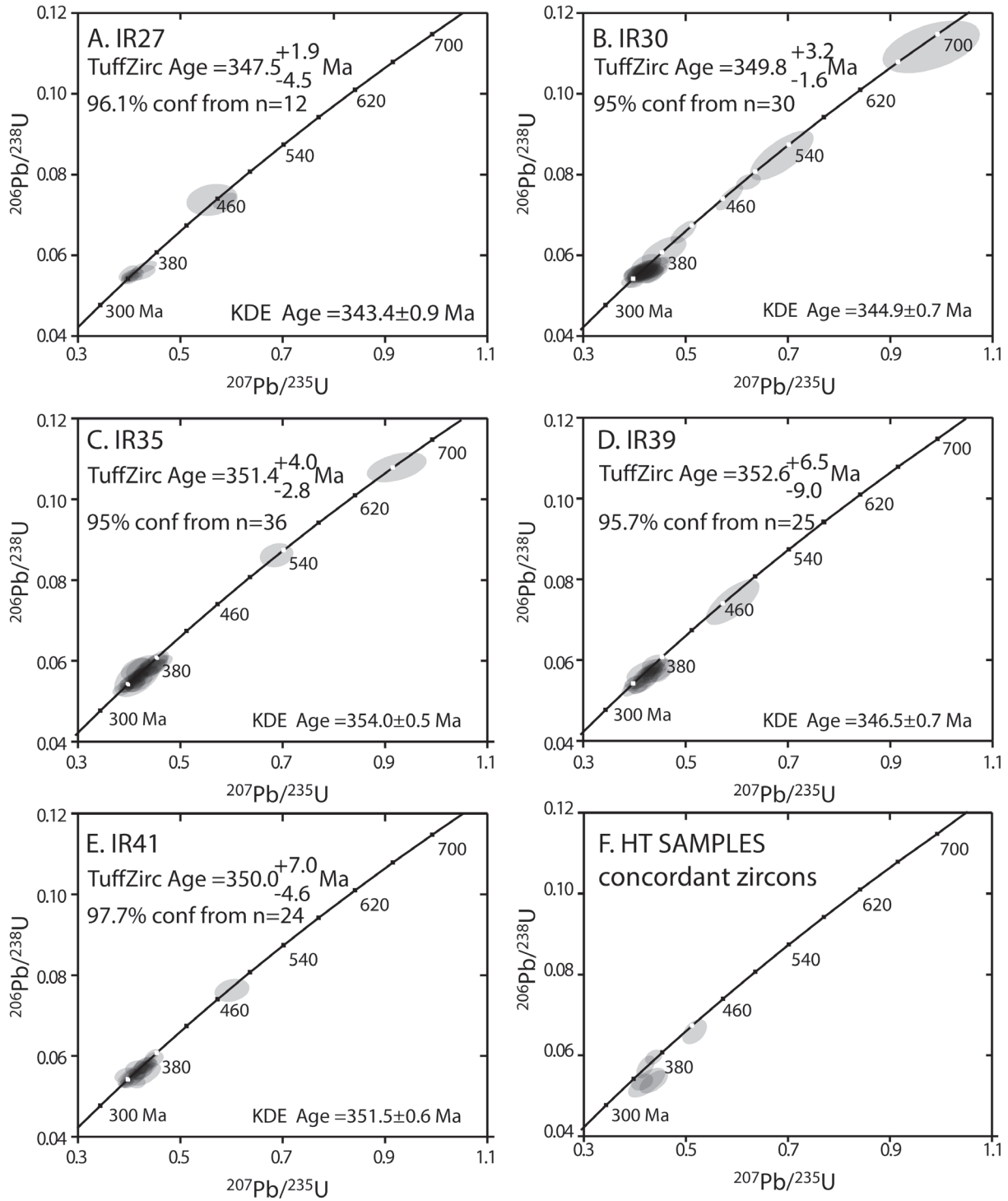


Fig. 8. U–Pb Concordia diagram of all zircons dated in this study for sample IR27 (A), IR30 (B), IR35 (C), IR39 (D), IR41 (E), and HT samples (F). We include the TuffZirc age, % confidence in the age, and the number of ages that define this confidence interval for the IR samples (Coutts et al. 2019).

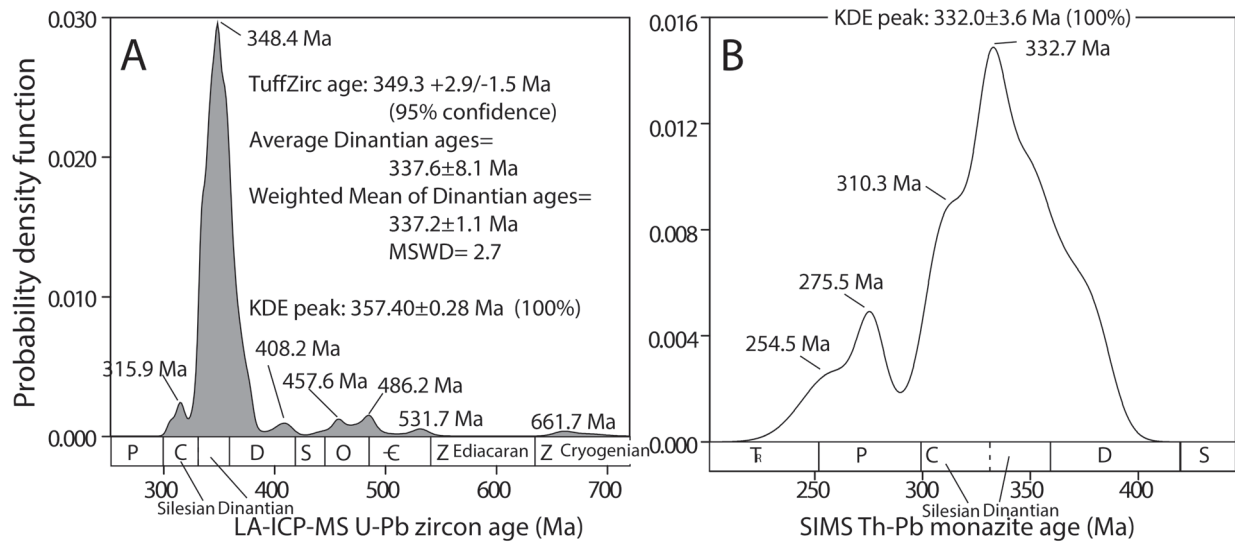


Fig. 9. Probability density diagrams showing the LA-ICP-MS age distribution of zircon ages (**A**) and SIMS monazite ages from granites dated in this study (**B**).

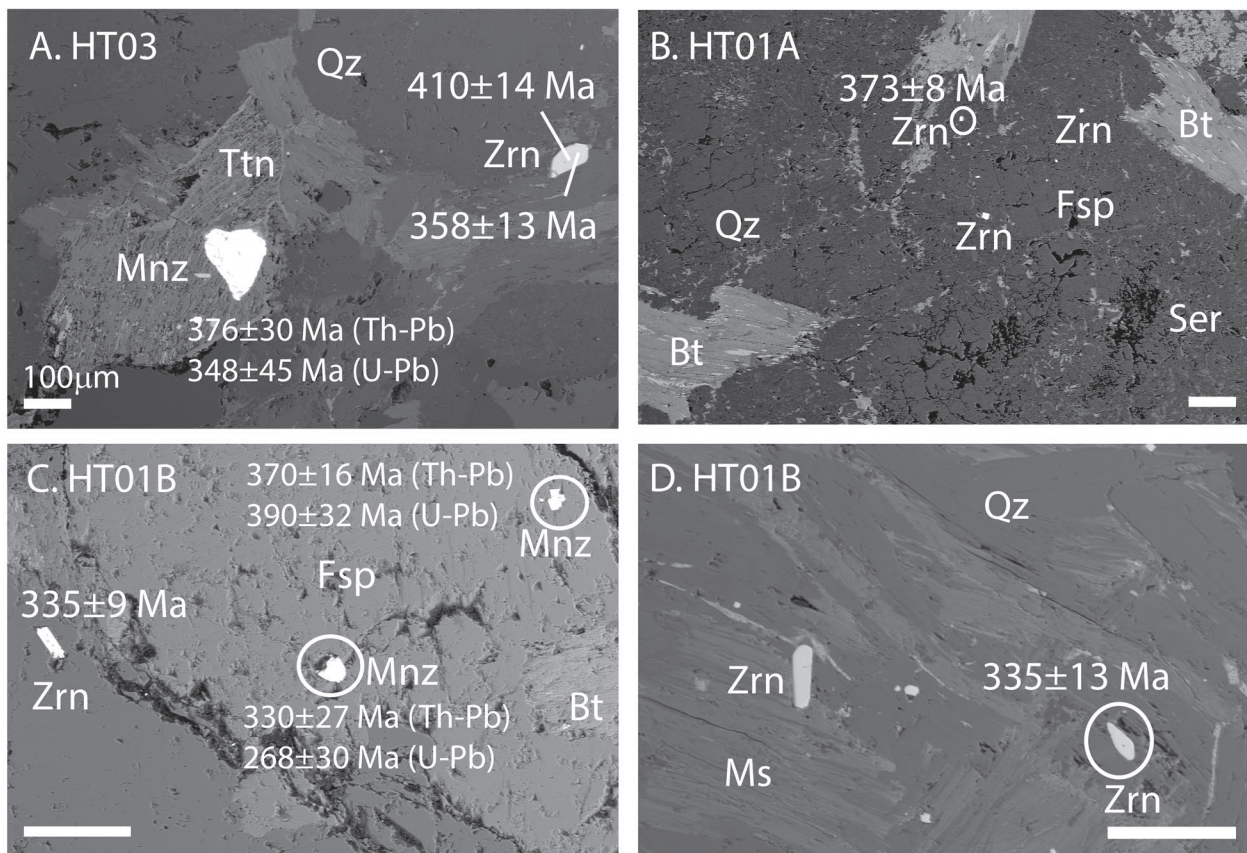


Fig. 10. BSE images of in situ dated monazite and zircon in situ in samples HT03 (**A**), HT01A (**B**), and HT01B (**C** and **D**). See Tables 4 and 5 and supplementary data for details regarding the ages. Mineral abbreviations here and elsewhere after Whitney & Evans (2010).

Discussion

Granitoid origin based on geochronology and geochemistry

Geochemical data from the granitoids are consistent with their emplacement in volcanic arc setting at lower P (<5 kbar) (Fig. 6D). The studied samples are peraluminous to strongly peraluminous with geochemical signatures that they derived from enriched mantle, non-garnet bearing source with some clay component (Figs. 5 and 6). This scenario is consistent with a vertically zoned, lower/middle crust consisting of older metagneous, amphibolitic, and metasedimentary rocks. Most granitoids appear to have a volcanic arc signature, except the

Baranec quartz monzonite sample (TT38) and High Tatra Mountains sample IR36 (Fig. 5B). These rocks also show similar HREE patterns, negative Eu anomalies, and a within plate granite (WPG) signature, suggesting the possible presence of melts from a collisional source are present in both regions (Figs. 6B, 7B and D). This observation is consistent with the trend observed in Fig. 6B and suggest the granitoids represent numerous magma injections and mixed felsic and mafic sources (Gawęda 2008; Burda et al. 2011; Gawęda & Szopa 2012; Szopa et al. 2013; Gawęda et al. 2016a). All samples are LREE enriched, and those with no or minor Eu anomalies are consistent with the moderately evolved nature of their melts with little or no fluid influence (Fig. 7).

The geochronological data provide a framework for understanding their magmatic history. Although Carboniferous ages dominate the number of zircon dates, the distribution of inheritance in Variscan intrusions is often employed to understand their tectonic and magmatic evolution (Tumiak et al. 2000; Chen et al. 2003; Friedl et al. 2004; Neiva et al. 2012; Broska et al. 2013; Fiannacca et al. 2019; Kohút & Larionov 2021). Inheritance patterns in igneous rocks are critical in relaying information regarding magma sources and petrogenetic processes (see review in Fiannacca et al. 2019).

The oldest zircon is in sample IR35 near Gerlachovský štít is 2544 ± 33 Ma and has an Early Carboniferous rim (343 ± 11 Ma). Although we have only one Paleoproterozoic/Neoproterozoic date from the High Tatra granites, its presence is significant in understanding the paleogeography of this region at older timeframes. The result appears similar to other Variscan-age magmatic assemblages that have an older Precambrian zircon signatures (Zeh et al. 2001; Friedl et al. 2004; Martin et al. 2018; Fiannacca et al. 2019; Schnapperelle et al. 2020). For example, zircons with Paleoproterozoic cores and Early Carboniferous rims are found in granitoids from the Austrian portion of the Bohemian Massif (Friedl et al. 2004) and the mid-German Crystalline Rise (Zeh et al. 2001) (Fig. 1A). The observation is consistent the origin of granites from the High Tatra Mountains as Variscan-age melts that have a component of recycled Proterozoic crust (e.g., Burda et al. 2013a,b).

Smaller LA-ICP-MS age peaks exist for granitoids in the High Tatra Mountains in the Cryogenian (661.7 Ma) and Cambrian (531.7 Ma) (Fig. 9). The age pattern is consistent with the observations of several intrusions within the western, central European

Variscan belt (Finger & Steyrer 1990; Franke 2000; Finger et al. 2009; Tichomirowa et al. 2019a,b). These include granites from Iberia to Armorica (NW France), Erzgebirge (Saxothuringian zone, Germany), the Bohemian Massif, the Brunovistulia, and Małopolska massifs (Czech Republic and southern Poland), and the crystalline massifs within the Alps, Carpathians, and extending to the Transcaucasian region in easternmost Europe (Fig. 1). These granites were emplaced during the Cambrian to Early Ordovician (510–480 Ma, Crowley et al. 2002; Gawęda et al. 2019) and subsequently re-melted or entrained xenocrystic zircon during the Variscan Orogeny (Matte 1998; Franke 2000; Seston et al. 2000; Dostal et al. 2019). The ages we report show little similarity in zircon ages extracted from sections of the Proto-Carpathian basement, which has been reported to be a long-lived magmatic arc that was active in earlier times (615–610 Ma) during the Timmanian/Baikalian rather than the Pan-African/Cadomian (Waśkowska et al. 2018; Gawęda et al. 2019). However, this terrane likely formed during distinct paleotectonic stages, and the Tatric and Veporic crystalline basements are thought to form a component of the Proto Tatric basement (Putiš et al. 2009; Broska et al. 2013; Gawęda et al. 2017; Burda et al. 2021).

The time frame for Variscan Orogeny-related deformation and metamorphism is suggested to have spanned from 480 Ma to 300–250 Ma (Gutiérrez-Alonso et al. 2008, 2011; Arenas et al. 2014; Kroner & Romer 2013; see review in Matte 2001; Casas & Murphy 2018; Dostal et al. 2019). Each dated sample yield TuffZirc and KDE ages that center ~350 Ma (Fig. 8). The TuffZirc representative date for all of the granitoid zircon LA-ICP-MS results is $349.3 \pm 2.9 / -1.5$ Ma. The most prominent peak on the PDD for the LA-ICP-MS zircon results is 348.8 Ma, which is younger than the more precise KDE peak of 357.40 ± 0.28 Ma. The most prominent peak on the PDD for the SIMS monazite ages is 332.7 Ma, which is similar to the KDE peak of 332.0 ± 3.6 Ma (Fig. 9).

Granites linked to S- and I/S-type magmatism are documented throughout the Variscan belt at ~350 Ma, which has been linked to crustal thickening, prograde metamorphism, and melting in the lower crust (Petrik et al. 1994; Tichomirowa et al. 2019a,b). The Tournaisian age reported here is found in other exposures of the core mountains, of which the High and Western Tatra Mountains are part (e.g., Kohút & Larionov 2021). In particular, the Central Western Carpathians records the Carboniferous S-type and I-type granitic series, which may overlap in their synchronous crystallization at 355–347 Ma (Kohút et al. 2009; Kohút & Larionov 2021). For example, the Strážovské vrchy Mountains has 348 Ma and 350 Ma ages (Kráľ et al. 1997) (Fig. 1). The zircon ages reported here are similar to zircon ages from the I/S-type granites from the Branisko Mountains (TuffZirc age $350.6 \pm 5.6 / -1.4$ Ma, $n=7$, 98.4 % confidence), Tribeč ($354.4 \pm 12.3 / -6.8$ Ma, $n=10$, 97.9 % confidence) and Žiar mountains ($348.2 \pm 6.2 / -8.9$ Ma, $n=11$, 93.5 % confidence) (Fig. 1) (Kohút & Larionov 2021).

Elsewhere, granitic assemblages in the Central Bohemian Plutonic Complex in the Czech Republic yield similar ages that were related to rapid and large-scale crustal extension in the Moldanubian zone (Holub et al. 1997). This time frame is also

consistent with large nappe stack thrusting at the northern margin of Gondwana in the Iberian margin (Catalán et al. 2009) and wrench faulting in the northern Massif Central in France (Leloix et al. 1999). The onset of extension in the central Europe and the Western Carpathians is broadly constrained to 340–260 Ma (Franke 2000; Hók et al. 2019).

The smaller 315.9 Ma age peak seen in the LA-ICP-MS zircon age results and the youngest Permian monazite ages would thus

correlate to extensional-related magmatism in the region (Fig. 9) (Lexa et al. 2003; Stampfli & Kozur 2006; Froitzheim et al. 2008; Tichomirowa et al. 2019a,b; Szemerédi et al. 2020; Villaseñor et al. 2021). Although the youngest zircon ages reported here are concordant, they could have experienced some degree of Pb loss that is not discernable based on their degree of concordance. Their smaller age peak in the probability diagram is similar, however, to estimates of the final collision, granite intrusion, and orogenic

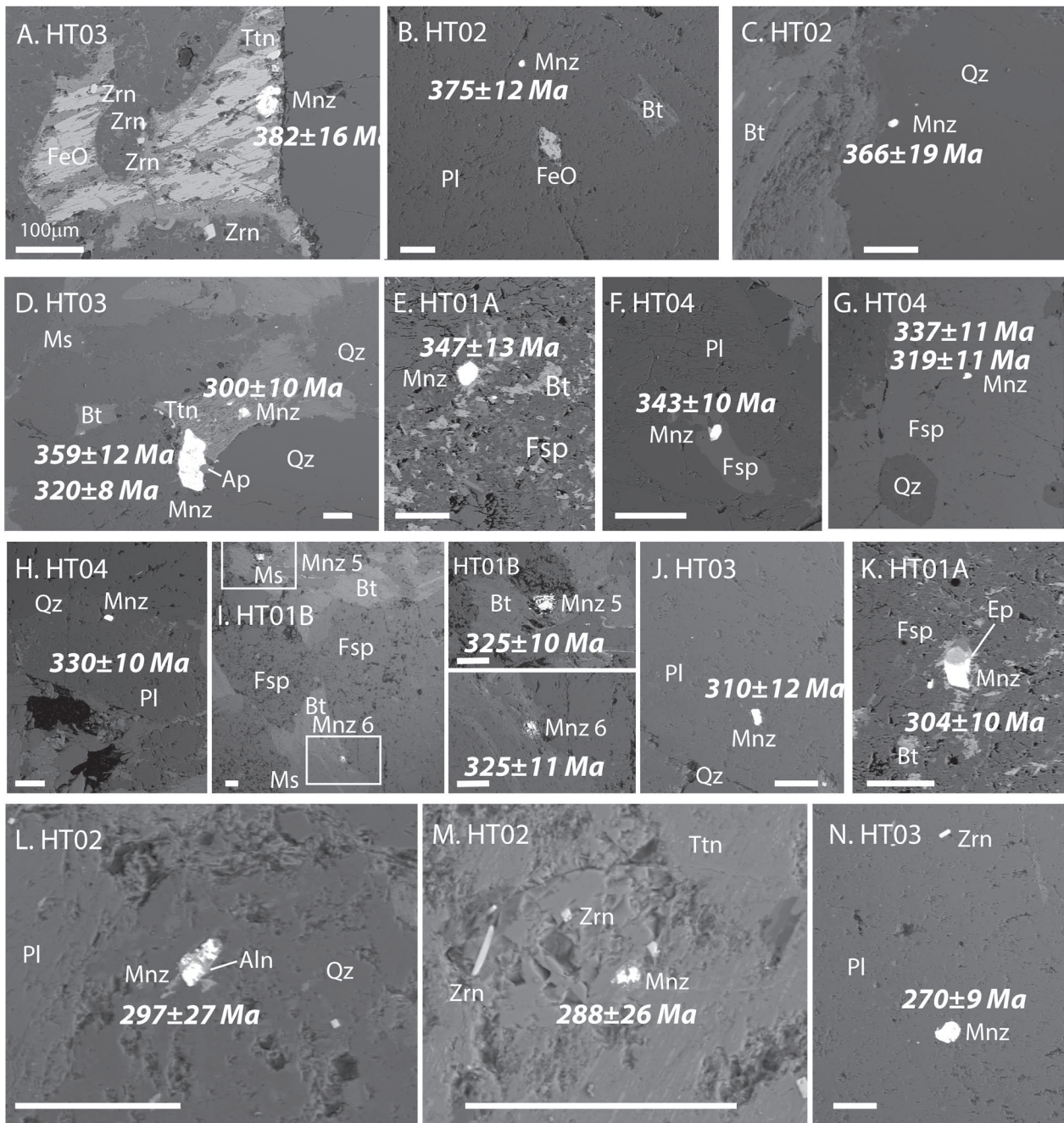


Fig. 11. BSE images of monazite grains dated in samples HT03 (A, D, J, and N), HT02 (B, C, L, and M), HT01A (E and K), HT04 (F, G, and H), and HT01B (I). Mineral abbreviations after Whitney & Evans (2010). Th–Pb monazite ages indicated. Images are arranged from oldest to youngest. See Table 5 and supplementary data for details regarding the ages.

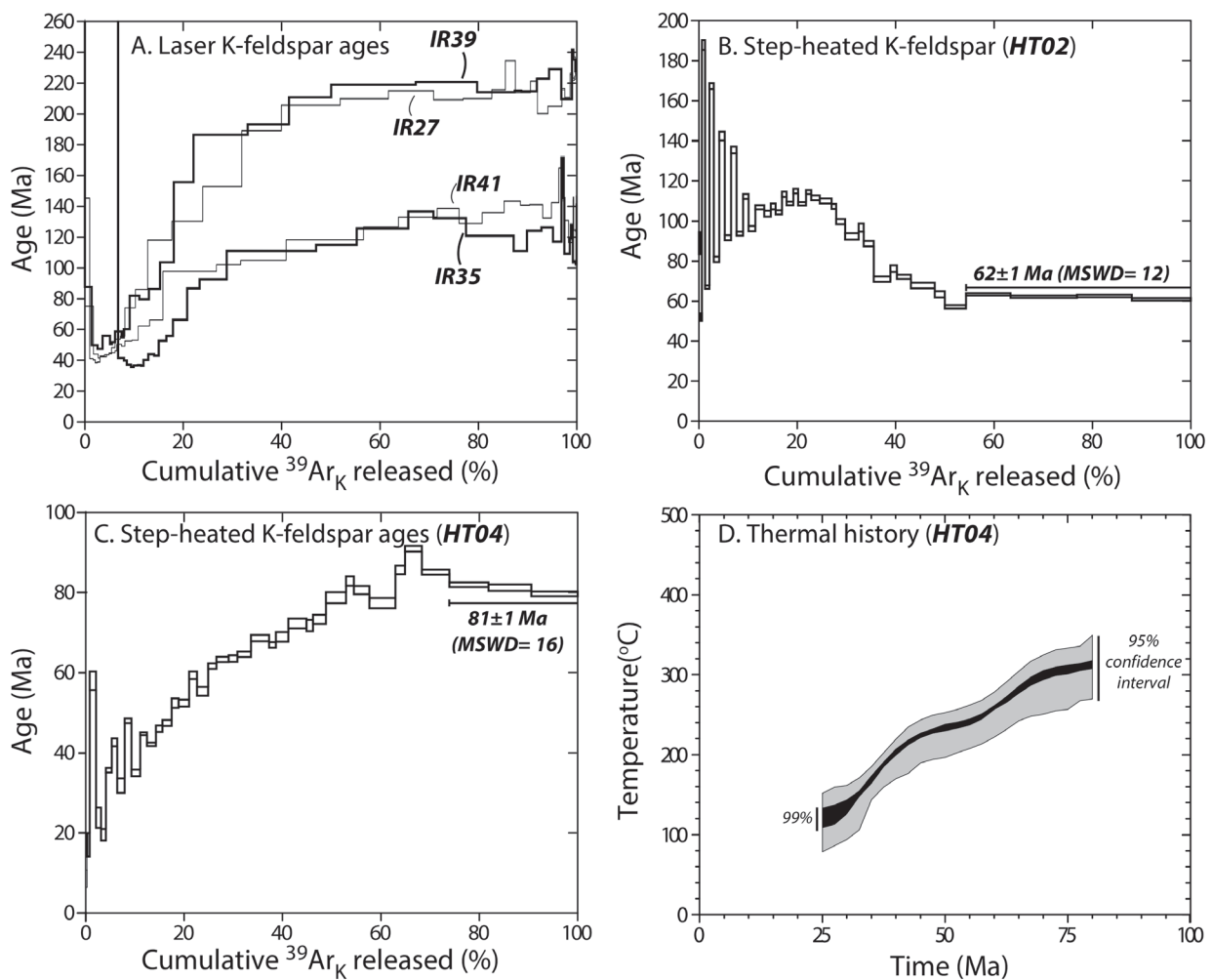


Fig. 12. A — K-feldspar $^{40}\text{Ar}/^{39}\text{Ar}$ ages (successive laser heating steps) from four High Tatra granites (IR39, IR27, IR35, and IR41). K-feldspar $^{40}\text{Ar}/^{39}\text{Ar}$ ages (generated using step-heating approach) from samples HT02 (B) and HT04 (C). Panel (D) shows the thermal history was extracted from sample HT04.

collapse in the Western and High Tatra Mountains timed at ca. 315 Ma (Poller & Todt 2000; Poller et al. 2001a). The younger 315.9 Ma LA-ICP-MS age peak is also consistent with when the Variscan hinterland of Western Europe was at a topographic high (Dusséaux et al. 2021).

The textural relationships of monazite dated in the granitoid assemblages suggest that they were likely affected by alteration or subsequent reactions (Figs. 10 and 11). For example, the titanite (CaTiSiO_5) seen in some BSE images of sample HT03 may be pseudomorph after allanite [$\text{Ca}_{1-x}(\text{REE}_x)(\text{Ti}, \text{Al}, \text{Fe})\text{SiO}_4(\text{O}, \text{OH}, \text{F})$], which contributed REE to crystallize monazite during alteration (Figs. 10A, 11A, D) (e.g., Broska et al. 2000; Catlos et al. 2002). Remnants of allanite or epidote are seen in sample HT02 (Fig. 11I, K, L). In these and other samples, allanite appears to fill cracks in plagioclase or feldspar (Figs. 10C, 11). The textures suggest that monazite likely appeared after allanite in these rocks and after crystallization, and was described in granitoids from the Tribeč Mts. (Broska et al. 2000).

Post-Variscan tectonics and implications for extrusion dynamics

K-feldspar $^{40}\text{Ar}/^{39}\text{Ar}$ ages suggest granitoids in the High Tatra Mountains track their exhumation history (Fig. 12). The oldest K-feldspar $^{40}\text{Ar}/^{39}\text{Ar}$ ages in samples IR27 and IR39 collected near Lomnický štít (Fig. 2C) are Late Triassic (~220 Ma). The time frame corresponds to the final stages of an episode of volcanism called the “*pietra verde*” found in the Southern Alps and the Transdanubian Range (Callegari & Monese 1964; Mundil et al. 1996; Harangi et al. 1996; Kohút et al. 2018; Dunkl et al. 2019). The cause of the volcanism remains enigmatic (see discussion in Kohút et al. 2018) is related to the either extensional-driven rifting or subduction related to the closure of an ocean unit south of the Inner Carpathian plate as the result of Early Cimmerian collision (e.g., Stampfli & Borel 2004; Schmid et al. 2020).

Sample IR35 and IR41 collected to the west of these rocks along the sub-Tatra fault and near Gerlachovský štít (Fig. 2C

and D) yielded younger Early Cretaceous $^{40}\text{Ar}/^{39}\text{Ar}$ ages in their last heating steps (~120 Ma). The sub-Tatra fault governs the present-day morphology of the Western and High Tatra Mountains and is overall a normal fault with a sub-vertical, or steeply south-dipping fault plane (Gross 1973; Gross et al. 1980; Maheľ 1986; Nemčok et al. 1993; Jurewicz 2006; Králiková et al. 2014). The structure may be one of a set of planar normal faults produced by tilt and spin rotations of domino-like prismatic upper crustal blocks that formed due to horizontal top-to the north simple shear of the Central Western Carpathian crust triggered by underthrusting of the Northern European plate (Grecula & Roth 1978; Marko 1995). Strike-slip motion is accommodated by the Ružbachy and Prosečné faults (Fig. 2A) that develop the Western and High Tatra Mountains into a compressional horst in a strike-slip duplex (Sperner 1996; Sperner et al. 2002). The age may represent the earliest timing of exhumation along the structure and correspond to events related to the re-arrangement of the Penninic-Austroalpine border zone from a passive to an active continental margin, which began at about 120 Ma (Wagreich 2001; Schuster et al. 2004).

Extrusion tectonics related to Alpine collision has long dominated ideas regarding the development of the Carpathians and the Western and High Tatra Mountains (Ratschbacher et al. 1991; Sperner et al. 2002; Schmid et al. 2008; Plašienka 2018a). The application of the idea is primarily the outcome of influential analog experiments by Ratschbacher et al. (1991) designed to simulate the conditions involved in the creation of the Eastern Alps that had a secondary impact on the creation of the Carpathian Mountains. Fundamental observations from the analog models suggest that weak lateral confinement, a broad and straight indenter, a narrow deformable area, and a rigid foreland best model structures within the Eastern Alps. An unconstrained and weak lateral boundary, a narrow deformable area, an area of high heat flow, and thin crust controls movement of wedges and favored lateral movement. The width of the indenter and size of the deformable area were responsible for determines the orientation of faults responsible for extrusion. Deformation is also thought to be accompanied by a migrating subduction zone of oceanic or thinned continental crust, creating the back-arc nature of the basin (e.g., Royden & Horvath 1988; Wortel & Spakman 2000; Márton et al. 2007). These observations are largely linked to the similar morphology seen in the Carpathian Mountains and the likewise arcuate shape of the Hellenic arc in the Aegean region and western Turkey (Fig. 1).

The external morphology of the Carpathians is thought to have developed due to the dense and regular fault network of mainly strike-slip and extensional structures within the Pannonian basin system as the ALCAPA and Tisza Dacia “mega-tectonic units” (Fig. 4) (e.g., Márton et al. 2007) that propagated into the free lateral boundary of the basin during Neogene (Ratschbacher et al. 1991; Hippolyte et al. 1999; Schmid et al. 2008; Lorinczi & Houseman, 2010; Kováč et al. 2107). The extrusion was also enhanced by subduction roll back along the northeastern margin (Royden 1993; Sperner et al. 2002; Seghedi et al. 2004; Schmid et al. 2008) or east-directed flux of asthenosphere or relative westward drift of the lithosphere (Doglioni et al. 1999).

The kinematic evolution of the Alps suggests that the Adriatic plate moved at a rate of 1.33 cm/yr between 65 and 50 Ma and 0.4 cm/yr during the Oligocene to the present (e.g., Schmid et al. 1996, 1997). Although these rates are significantly slower than the indenter velocities chosen by Ratschbacher et al. (1991) analog models, subsequent experiments have shown the importance of weak lateral confinement in developing the Carpathian Mountains (e.g., Royden 1993; van Gelder et al. 2017) and the rotation of specific blocks within the extruding portion (e.g., Rauch 2013). In the Outer Carpathians, the timing of the last episode of thrusting is suggested to have migrated eastward from the Early Miocene to Plio–Pleistocene.

Although the last significant exhumation pulse for the High Tatra Mountains is assumed to have occurred during the Middle Miocene (Fig. 4), K-feldspar $^{40}\text{Ar}/^{39}\text{Ar}$ ages from granitic rocks yield Eocene (40.8 ± 0.3 Ma) results from their initial degassing steps (Fig. 12A). We suggest these ages time when the mineral passed through a ~150 °C geotherm (depending on grain size and cooling rate). The ages are consistent with previously reported Eocene (U–Th)/He zircon ages from similar assemblages (Anczkiewicz et al. 2015; Śmigielski et al. 2016), but are much older than the sedimentary rock record of the accretionary wedge in the Outer Carpathians that would predict ~20 Myr younger results (Fig. 4) (Săndulescu 1988; Csontos et al. 1992; Plašienka 2018a). However, the Eocene $^{40}\text{Ar}/^{39}\text{Ar}$ K-feldspar ages correspond well with limited sedimentological data that proposed that the process of tectonic escape initiated in the Eocene (Fodor et al. 1992). Eocene (Bartonian)–Late Oligocene deposits are also present in sediments in the Liptov Basin, south of the range (Fig. 2) (e.g., Starek et al. 2019).

The $^{40}\text{Ar}/^{39}\text{Ar}$ K-feldspar thermal history extracted from sample HT04 at the base of Lomnický štít was allows for the possibility that exhumation rates may have proceeded at faster rates between 70–55 Ma and from 45–25 Ma (Fig. 12D). This time frame is attributed to a change from extensional tectonics to transpression and transtension during the Late Paleocene to Eocene (~80–45 Ma) (Králiková et al. 2014). Thermal modeling suggests that sample HT04 was at the ~100 °C isotherm by 25 Ma. The plateau age $^{40}\text{Ar}/^{39}\text{Ar}$ K-feldspar ages from sample HT02 from the top of Lomnický štít from the final steps is 62 ± 1 Ma, but the age patterns show it is affected by excess argon. This type of thermal modeling from more samples is helpful for understanding the exhumation history of the range and should be pursued in developing future models for its exhumation.

Conclusions

The Western and High Tatra Mountains are a major uplifted component of the Western Carpathian basement. They are a logical location to study arcuate orogenesis, exhumation rates of the deep crust, and magnitudes and rates involved in the transfer of heat and mass during mountain-building events. Deciphering the tectonic events recorded in the Western Carpathian region is an essential component for global plate reconstructions and understanding how the range links to other locales that document

the closure of Tethyan oceans throughout Europe. We present geochemical and geochronological data from the High Tatra Mountains and Baranec massif in the Western Carpathians that have significant implications on our understanding of their development and models for extrusion tectonics for the region.

Geochemical data from samples from the Western and High Tatra Mountains suggest they were emplaced in a volcanic arc setting at lower P (<5 kbar), and most have been derived from a mafic source, enriched mantle, non-garnet bearing source with some clay component. Only two from the Western Tatra Mountains sample and High Tatra Mountains have HREE patterns and negative Eu anomalies that show a WPG signature, suggesting the presence of melts from a collisional source are present in both regions.

Zircon ages suggest significant crystallization at ~350 Ma, but the presence of the older Neoproterozoic to Ordovician inherited ages are common and match those reported for Variscan igneous assemblages throughout Europe. These ages link these rocks to I/S-type magmatism documented throughout the Variscan belt at this time, characterized by a source in vertically zoned lower crust consisting of old metagneous, amphibolitic, and metasedimentary rocks. In addition, the presence of Permian monazite ages indicates the range was not immune from the wide-scale extensional dynamics that affected the region during this time.

Younger ages obtained using K-feldspar $^{40}\text{Ar}/^{39}\text{Ar}$ thermochronology are consistent with the granitoids experiencing slow cooling. The older ages indicate that the region experienced uplift much earlier (Late Cretaceous) than predicted by models of extrusion tectonics often applied to the region. Pulses of exhumation characterize the thermal history from K-feldspar from a granitoid collected at the base of Lomnický štít, and thermal modeling of this rock suggests it cooled from ~300 °C to ~100 °C from ~78 Ma to 25 Ma, but at faster rates at intervals between 70–55 Ma and 45–35 Ma. The youngest $^{40}\text{Ar}/^{39}\text{Ar}$ K-feldspar ages from all samples dated using laser step-heating average 40.8 ± 0.3 Ma and are consistent with ALCAPA escape followed by Alpine uplift in stages. These ages and the thermal history are important constraints on timing the development of the Carpathian arc, and suggest additional complexity within specific segments in the range.

Acknowledgments: This work was supported by the National Science Foundation (NSF), grant number 1460050. IB and MK were supported by the Slovak Research and Development Agency, grant number APVV-18-0107 and VEGA 2/0075/20. We appreciate field assistance and discussions with Brent A. Elliott, Thomas Quintero, Theresa Perez, Saloni Tandon, and Zoe Yin. Dušan Catlos, Miro Hreus, and Karol Ivanič assisted with the collection of the HT assemblages. We appreciate analytical assistance from Lisa Stockli at the UT Austin (U–Th)/He and U–Pb Geo-Thermochronometry Lab. The ion microprobe facility at UCLA is partly supported by a grant from the Instrumentation and Facilities Program, Division of Earth Sciences, NSF. We appreciate drafting assistance from Jeffrey Horowitz (Dept. Geological Sciences, Jackson School, UT Austin) and assistance with

the argon geochronology from Marty Grove (Stanford University). Data supporting the conclusions of this paper is publicly available as supplementary files. Comments from Edyta Jurewicz and an anonymous reviewer greatly improved the original manuscript.

References

- Anczkiewicz A.A., Środoń J. & Zattin M. 2013: Thermal history of the Podhale Basin in the internal Western Carpathians from the perspective of apatite fission track analyses. *Geologica Carpathica* 642, 141–151. <https://doi.org/10.2478/geoca-2013-0010>
- Anczkiewicz A.A., Danišik M. & Środoń J. 2015: Multiple low-temperature thermochronology constraints on exhumation of the Tatra Mountains: New implication for the complex evolution of the Western Carpathians in the Cenozoic. *Tectonics* 34, 2296–2317. <https://doi.org/10.1002/2015TC003952>
- Andrusov D. 1968: Grundriss der Tektonik der Nördlichen Karpaten. *Verlag der Slowakischen Akademie der Wissenschaften, Bratislava*, 1–188.
- Arenas R., Fernández R.D., Martínez S.S., Gerdes A., Fernández-Suárez J. & Albert R. 2014: Two-stage collision: Exploring the birth of Pangea in the Variscan terranes. *Gondwana Research* 25, 756–763. <https://doi.org/10.1016/j.gr.2013.08.009>
- Baumgart-Kotarba M., Marcak H. & Marton E. 2004: Rotation along the transverse transforming Orava strike-slip fault; based on geomorphological, geophysical and paleomagnetic data; western Carpathians. *Geologica Carpathica* 55, 219–226.
- Bea F. 1996: Residence of REE, Y, Th and U in granites and crustal protoliths; Implications for the chemistry of crustal melts. *Journal of Petrology* 37, 521–552. <https://doi.org/10.1093/ptrology/37.3.521>
- Bezák V., Biely A., Elečko M., Konečný V., Mello J., Polák M. & Potfaj M. 2011: A new synthesis of the geological structure of Slovakia - the general geological map at 1:200 000 scale. *Geological Quarterly* 55, 1–8.
- Blevin P.L. 2004: Metallogeny of granitic rocks. In: The Ishihara Symposium: Granites and Associated Metallogenesis. *Geoscience Australia*, 1–4. http://www.ga.gov.au/webtemp/image_cache/GA3671.pdf
- Bowring S.A., Schoene B., Crowley J.L., Ramezani J. & Condon, D.J. 2006: High-precision zircon U–Pb geochronology and the stratigraphic record: Progress and promise. In: Olszewski T. (Ed.): *Geochronology: Emerging Opportunities. Paleontological Society Short Course* 11, 23–45. <https://doi.org/10.1017/S1089332600001339>
- Broska I., Janák M., Svojtka M., Yi K., Konečný P., Kubiš M., Kurylo S., Hrdlička M. & Maraszewska M. 2022: Variscan granitic magmatism in the Western Carpathians with linkage to slab break-off. *Lithos* 412–413, 106589
- Broska I., Petrik I. & Williams C.T. 2000: Coexisting monazite and allanite in peraluminous granitoids of the Tribeč Mountains, Western Carpathians. *American Mineralogist* 85, 22–32. <https://doi.org/10.2138/am-2000-0104>
- Broska I., Petrik I., Be'eri-Shlevin Y., Majka J. & Bezák V. 2013: Devonian/Mississippian I-type granitoids in the Western Carpathians: A subduction-related hybrid magmatism. *Lithos* 162–163, 27–36. <https://doi.org/10.1016/j.lithos.2012.12.014>
- Broska I. & Svojtka M. 2020: Early Carboniferous successive I/S-type granite magmatism recorded in the Malá Fatra Mountains by LA ICP-MS zircon dating (Western Carpathians). *Geologica Carpathica* 71, 391–401. <https://doi.org/10.31577/GeolCarp.71.5.1>
- Burchart J. 1968: Rubidium-strontium isochron ages of the crystalline core of the Tatra Mts. Poland. *American Journal of Science* 266, 895–907

- Burda J. & Klötzli U. 2007: First report of LA-ICP-MS U–Pb geochronology of the Goryczkowa type granite (Tatra Mountains), Poland. *Mitteilungen der Österreichischen Mineralogischen Gesellschaft* 153.
- Burda J. & Klötzli U. 2011: Pre-Variscan evolution of the western Tatra Mountains; new insights from U–Pb zircon dating. In: Broska I., Finger F. & Harlov D.E. (Eds.): Accessory minerals in igneous and metamorphic rocks. *Mineralogy and Petrology* 102, 99–115.
- Burda J., Gawęda A. & Klötzli U. 2011: Magma hybridization in the Western Tatra Mts. granitoid intrusion (S-Poland, Western Carpathians). *Mineralogy and Petrology* 103, 19–36. <https://doi.org/10.1007/s00710-011-0150-1>
- Burda J., Gawęda A. & Klötzli U. 2013a: U–Pb zircon age of the youngest magmatic activity in the High Tatra granites Central Western Carpathians. *Geochronometria* 40, 134–144.
- Burda J., Gawęda A. & Klötzli U. 2013b: Geochronology and petrogenesis of granitoid rocks from the Goryczkowa Unit, Tatra Mountains central Western Carpathians. *Geologica Carpathica* 64, 419–435. <https://doi.org/10.2478/geoca-2013-0029>
- Burda J., Klötzli U., Majka J., Chew D., Li Q-L., Liu Y., Gawęda A. & Wiedenbeck M. 2021: Tracing proto-Rheic – Qaidam Ocean vestiges into the Western Tatra Mountains and implications for the Palaeozoic palaeogeography of Central Europe. *Gondwana Research* 91, 188–204. <https://doi.org/10.1016/j.gr.2020.12.016>
- Callegari E. & Monese A. 1964: Il chimismo della “pietra verde” degli Strati di Livinallongo (Dolomiti): Contributo allo studio petrogenetico della “pietra verde” ladinica. *Studi Trentini di Scienze Naturali Trento* 41, 45–71.
- Carey S.W. 1955: The orocline concept in geotectonics – Part I. *Papers and Proceedings of the Royal Society of Tasmania* 89, 255–288.
- Casas J.M. & Murphy J.B. 2018: Unfolding the arc: The use of pre-orogenic constraints to assess the evolution of the Variscan belt in Western Europe. *Tectonophysics* 736, 47–61. <https://doi.org/10.1016/j.tecto.2018.04.012>
- Castelluccio A., Andreucci B., Zattin M., Ketcham R.A., Jankowski L., Mazzoli S. & Szaniawski R. 2015: Coupling sequential restoration of balanced cross sections and low temperature thermochronometry: The case study of the Western Carpathians. *Lithosphere* 7, 367–378. <https://doi.org/10.1130/L436.1>
- Catalán J.R.M., Arenas R., Abati J., Martínez S.S., García F.D., Suárez J.F., Cuadra P.G., Castiñeiras P., Barreiro J.G., Montes A.D., Clavijo E.G., Pascual, F.J.R., Andonaegui P., Jeffries T.E., Alcock J.E., Fernández R.D. & Carmona A.L. 2009: A rootless suture and the loss of the roots of a mountain chain: the Variscan belt of NW Iberia. *Comptes Rendus Geoscience* 341, 114–126.
- Catlos E.J. 2013: Versatile Monazite: resolving geological records and solving challenges in materials science: Generalizations about monazite: Implications for geochronologic studies. *American Mineralogist* 98, 819–832. <https://doi.org/10.2138/am.2013.4336>
- Catlos E.J. & Miller N.R. 2016: Ion microprobe ^{208}Th – ^{208}Pb ages from high common Pb monazite, Morefield Mine, Amelia County, Virginia: Implications for Alleghanian tectonics. *American Journal of Science* 316, 470–503. <https://doi.org/10.2475/05.2016.03>
- Catlos E.J., Gilley L.D. & Harrison T.M. 2002: Interpretation of monazite ages obtained via in situ analysis. *Chemical Geology* 188, 193–215.
- Catlos E.J., Jacob L., Oyman T. & Sorensen S. 2012. Long-term exhumation of an Aegean metamorphic core complex granitoids in the Northern Menderes Massif, western Turkey. *American Journal of Science* 312, 534–571. <https://doi.org/10.2475/05.2012.03>
- Catlos E.J., Mark D.F., Suarez S., Brookfield M.E., Miller C.G., Schmitt A.K., Gallagher V. & Kelly A. 2020: Late Silurian zircon U–Pb ages from the Ludlow and Downton bone beds, Welsh Basin, UK. *Journal of the Geological Society* 178, jgs2020-107. <https://doi.org/10.1144/jgs2020-107>
- Chen F., Chen F., Siebel W. & Satir M. 2003: Geochemical and isotopic composition and inherited zircon ages as evidence for lower crustal origin of two Variscan S-type granites in the NW Bohemian massif. *International Journal of Earth Science* 92, 173–184. <https://doi.org/10.1007/s00531-003-0310-6>
- Chorowicz J. 2016: Genesis of the Pieniny Klippen Belt in the Carpathians: Possible effects of a major paleotransform fault in the Neo-Tethyan domain. *Comptes Rendus Geoscience* 348, 15–22.
- Cifelli F., Caricchi C. & Mattei M. 2016: Formation of arc-shaped orogenic belts in the Western and Central Mediterranean: A palaeomagnetic review. *Geological Society London Special Publications* 425, 37–63. <https://doi.org/10.1144/SP425.12>
- Coutts D.S., Matthews W.A. & Hubbard S.M. 2019: Assessment of widely used methods to derive depositional ages from detrital zircon populations. *Geoscience Frontiers* 10, 1421–1435. <https://doi.org/10.1016/j.gsf.2018.11.002>
- Crowley Q.G., Floyd P.A., Štědrá V., Winchester J.A., Kachlík V. & Holland J.G. 2002: The Mariánské-Lázně Complex, NW Bohemian Massif: development and destruction of an early Palaeozoic seaway. *Geological Society, London, Special Publications* 201, 177–195. <https://doi.org/10.1144/GSL.SP.2002.201.01.09>
- Csontos L. & Vörös A. 2004: Mesozoic plate tectonic reconstruction of the Carpathian region. *Palaeogeography, Palaeoclimatology, Palaeoecology* 210, 1–56.
- Csontos L., Nagymarosy A., Horváth F. & Kováč M. 1992: Tertiary evolution of the Intra Carpathian area: A model. *Tectonophysics* 208, 221–241. [https://doi.org/10.1016/0040-1951\(92\)90346-8](https://doi.org/10.1016/0040-1951(92)90346-8)
- Decker K. 1996: Miocene tectonics at the Alpine–Carpathian junction and the evolution of the Vienna basin. *Mitteilungen der Gesellschaft der Geologie- und Bergbaustudenten in Österreich* 41, 33–44.
- Dogliani C., Harabaglia P., Merlini S., Mongelli F., Peccerillo A. & Piromallo C. 1999: Orogens and slabs vs. their direction of subduction. *Earth-Science Reviews* 45, 167–208. [https://doi.org/10.1016/S0012-8252\(98\)00045-2](https://doi.org/10.1016/S0012-8252(98)00045-2)
- Dostal J., Murphy J.B., Shellnutt J.G., Ulrych J. & Fediuk F. 2019: Neoproterozoic to Cenozoic magmatism in the central part of the Bohemian Massif Czech Republic: Isotopic tracking of the evolution of the mantle through the Variscan orogeny. *Lithos* 326–327, 358–369. <https://doi.org/10.1016/j.lithos.2018.12.028>
- Dunkl I., Farics É., Józsa S., Lukács R., Haas J. & Budai T. 2019: Traces of Carnian volcanic activity in the Transdanubian I Range, Hungary. *International Journal of Earth Sciences* 108, 1451–1466.
- Dusséaux C., Gébélín A., Ruffet G. & Mulch A. 2021: Late Carboniferous paleoelevation of the Variscan Belt of Western Europe. *Earth and Planetary Science Letters* 569, 117064. <https://doi.org/10.1016/j.epsl.2021.117064>
- Fiannacca P., Williams I.S., Cirrincione R. & Pezzino A. 2019: Poly-orogenic melting of metasedimentary crust from a granite geochemistry and inherited zircon perspective (Southern Calabria–Peloritani Orogen, Italy). *Frontiers in Earth Science* 7. <https://www.frontiersin.org/article/10.3389/feart.2019.00119>
- Finger F. & Steyrer H.P. 1990: I-type granitoids as indicators of a late Paleozoic convergent ocean-continent margin along the southern flank of the central European Variscan orogen. *Geology* 18, 1207–1210. [https://doi.org/10.1130/0091-7613\(1990\)018%3C1207:ITGAIO%3E2.3.CO;2](https://doi.org/10.1130/0091-7613(1990)018%3C1207:ITGAIO%3E2.3.CO;2)
- Finger F., Gerdes A., René M. & Riegler G. 2009: The Saxo-Danubian Granite Belt: magmatic response to postcollisional delami-

- nation of mantle lithosphere below the southwestern sector of the Bohemian Massif (Variscan orogen). *Geologica Carpathica* 60, 205–212. <https://doi.org/10.2478/v10096-009-0014-3>
- Fodor L., Magyari A., Kázmér M. & Fogaras A. 1992: Gravity-flow dominated sedimentation on the Buda paleoslope Hungary: Record of Late Eocene continental escape of the Bakony unit. *Geologische Rundschau* 81, 695–716.
- Franke W. 2000: The mid-European segment of the Variscides: tectonostratigraphic units, terrane boundaries and plate tectonic evolution. In: Franke W., Haak V., Oncken O. & Tanner D. (Eds): *Orogenic processes: Quantification and modelling in the Variscan Belt. Geological Society, London, Special Publications* 179, 35–61.
- Friedl G., Finger F., Paquette J.L., von Quadt A., McNaughton N.J. & Fletcher I.R. 2004: Pre-Variscan geological events in the Austrian part of the Bohemian Massif deduced from U–Pb zircon ages. *International Journal of Earth Science* 93, 802–823. <https://doi.org/10.1007/s00531-004-0420-9>
- Froitzheim N., Plašienka D. & Schuster R. 2008: Alpine tectonics of the Alps and Western Carpathians. In: McCann T. (Ed.): *The Geology of Central Europe. The Geological Society*, 2. <https://doi.org/10.1144/CEV2P.6>
- Frost B.R., Barnes C.G., Collins W.J., Arculus R.J., Ellis D.J. & Frost C.D. 2001: A Geochemical Classification for Granitic Rocks. *Journal of Petrology* 42, 2033–2048. <https://doi.org/10.1093/ptetrology/42.11.2033>
- Gągała L., Vergés J., Saura E., Malata T., Ringenbach J.-C., Werner P. & Krzywiec P. 2012: Architecture and orogenic evolution of the northeastern Outer Carpathians from cross-section balancing and forward modeling. *Tectonophysics* 532–535, 223–241. <https://doi.org/10.1016/j.tecto.2012.02.014>
- Gawęda A. 1995: Geochemistry and Rb/Sr isochron age of pegmatites from the Western Tatra Mts. *Geologica Carpathica* 46, 95–99.
- Gawęda A. 2007: Variscan granitoid magmatism in Tatra Mountains – the history of subduction and continental collision. In: Kozłowski A., Wiszniewska J. (Eds.): *Granitoids in Poland. AM Monograph* 1, 319–332.
- Gawęda A. 2008: Apatite-rich enclave in the High Tatra granite, Western Carpathians: petrological and geochronological study. *Geologica Carpathica* 59, 295–306.
- Gawęda A. & Szopa K. 2012: The origin of magmatic layering in the High Tatra granite, Central Western Carpathians – implications for the formation of granitoid plutons. *Earth Environmental Science Transactions of the Royal Society of Edinburgh* 103, 129–144. <https://doi.org/10.1017/S1755691012010146>
- Gawęda A., Kozłowski K. & Piotrowska K. 1998: Tectonic development of the crystalline basement of the Polish part of the Western Tatra Mts. *Acta Universitatis Carolinae, Geologica* 42, 252–253.
- Gawęda A., Winchester J.A., Kozłowski K., Narębski W. & Holland J.G. 2000: Geochemistry and palaeotectonic setting of amphibolites from the Western Tatra Mountains, southern Poland. *Geological Journal* 35, 69–85.
- Gawęda A., Szopa K. & Chew D. 2014: LA-ICP-MS U–Pb dating and REE patterns of apatite from the Tatra Mountains, Poland as a monitor of the regional tectonomagmatic activity. *Geochronometria* 41, 306–314.
- Gawęda A., Szopa K., Chew D., Klötzli U., Müller A., Sikorska M. & Pyka P. 2016a: Age and origin of fluorapatite-rich dyke from Baranec Mt. (Tatra Mts. Western Carpathians): a key to understanding of the post-orogenic processes and element mobility. *Geologica Carpathica* 67, 417–432. <https://doi.org/10.1515/geoca-2016-0026>
- Gawęda A., Burda J., Klötzli U., Golonka J. & Szopa K. 2016b: Episodic construction of the Tatra granitoid intrusion Central Western Carpathians, Poland/Slovakia: consequences for the geodynamics of Variscan collision and Rheic Ocean closure. *International Journal of Earth Sciences* 105, 1153–1174. <https://doi.org/10.1007/s00531-015-1239-2>
- Gawęda A., Burda J., Golonka J., Klötzli U., Chew D., Szopa K. & Wiedenbeck M. 2017: The evolution of eastern Tornquist-Paleoasian Ocean and subsequent continental collisions: A case study from the Western Tatra Mountains, Central Western Carpathians (Poland). *Gondwana Research* 48, 134–52.
- Gawęda A., Szopa K., Chew D., O’Sullivan G.J., Burda J., Klötzli U. & Golonka J. 2018: Variscan post-collisional cooling and uplift of the Tatra Mountains crystalline block constrained by integrated zircon, apatite and titanite LA-(MC)-ICP-MS U–Pb dating and rare earth element analyses. *Chemical Geology* 484, 191–209. <https://doi.org/10.1016/j.chemgeo.2018.03.012>
- Gawęda A., Szopa K., Włodyka R., Burda J., Crowley Q. & Sikorska M. 2019: Continuous magma mixing and cumulate separation in the High Tatra Mountains open system granitoid intrusion, Western Carpathians Poland/Slovakia: a textural and geochemical study. *Acta Geologica Polonica* 4, 549–570. <https://doi.org/10.24425/agp.2019.126447>
- Gehrels G. 2012: Detrital zircon U–Pb geochronology: current methods and new opportunities. In: Busby C. & Azor A. (Eds.): *Tectonics of Sedimentary Basins: Recent Advances, First Edition. Blackwell Publishing Ltd.*, 47–62.
- Golonka J., Krobicki M., Pajak J., Giang N. V. & Zuchiewicz W. 2006: Global plate tectonics and paleogeography of Southeast Asia. *Faculty of Geology, Geophysics and Environmental Protection, AGH University of Science and Technology, Arkadia, Kraków*, 1–128.
- Grecl P. & Roth Z. 1978: Kinematic model of the West Carpathians. *Sborník Geologických Věd, Geologie*, 49–73.
- Gross P. 1973: On the character of the Choč-sub-Tatra fault. *Geologické Práce Správy* 61, 315–319 (in Slovak).
- Gross P., Köhler E., Biely A., Franko O., Hanzel V., Hricko J., Kupčo G., Papšová J., Priečovská Z., Szalaiová V., Snopková P., Stránska M., Vaškovič I. & Zbořil 1980: Geology of the Liptovská kotlina Basin. *GÚDŠ, Bratislava*, 1–242 (in Slovak).
- Gutiérrez-Alonso G., Fernández-Suárez J., Weil A.B., Murphy J.B., Nance R.D., Corfu F. & Johnston S.T. 2008: Self-subduction of the Pangaeon global plate. *Nature Geoscience* 1, 549–553. <https://doi.org/10.1038/ngeo250>
- Gutiérrez-Alonso G., Murphy J.B., Fernández-Suárez J., Franco M.P., Gonzalo J.C. & Weil A.B. 2011: Lithospheric mantle replacement in the core of Pangea: Sm–Nd insights from Iberia. *Geology* 39, 155–158.
- Harangi S., Szabó C., Józsa S., Szoldán Z., Árvás-Sós E., Balla M. & Kubovics I. 1996: Mesozoic igneous suites in Hungary: implications for genesis and tectonic setting in the Northwestern Part of Tethys. *International Geology Reviews* 38, 336–360. <https://doi.org/10.1080/00206819709465339>
- Harrison T.M. & Lovera O.M. 2013: The multi-diffusion domain model: past, present and future. *Geological Society, London, Special Publications* 378, 91–106. <https://doi.org/10.1144/SP378.9>
- Harrison T.M., Grove M., Mckeegan K.D., Coath C.D., Lovera O.M. & Le Fort P. 1999: Origin and episodic emplacement of the Manaslu Intrusive Complex, Central Himalaya. *Journal of Petrology* 40, 3–19. <https://doi.org/10.1093/ptetroj/40.1.3>
- Hecht L., Thuro K., Plinninger R. & Cuney M. 1999: Mineralogical and geochemical characteristics of hydrothermal alteration and episyenitization in the Königshain granites, northern Bohemian Massif, Germany. *International Journal of Earth Sciences* 88, 236–252. <https://doi.org/10.1007/s005310050262>
- Heilimo E., Halla J. & Hölttä P. 2010: Discrimination and origin of the Sanukitoid series: Geochemical constraints from the Neoar-

- chean western Karelian Province Finland. *Lithos* 115, 27–39. <https://doi.org/10.1016/j.lithos.2009.11.001>
- Herriott T.M., Crowley J.L., Schmitz M.D., Wartes M.A. & Gillis R.J. 2019: Exploring the law of detrital zircon: LA-ICP-MS and CA-TIMS geochronology of Jurassic forearc strata, Cook Inlet, Alaska, USA. *Geology* 47, 1044–1048. <https://doi.org/10.1130/G46312.1>
- Hippolyte J.C., Badescu D. & Constantin P. 1999: Evolution of the transport direction of the Carpathian belt during its collision with the east European Platform. *Tectonics* 18, 11201138.
- Hók J., Pelech O., Teták F., Németh Z. & Nagy A. 2019: Outline of the geology of Slovakia W. Carpathians. *Mineralia Slovaca* 51, 31–60.
- Holub F.V., Cocherie A. & Rossi P. 1997: Radiometric dating of granitic rocks from the Central Bohemian Plutonic Complex Czech Republic: constraints on the chronology of thermal and tectonic events along the Moldanubian–Barrandian boundary. *Comptes Rendus de l'Académie des Sciences – Series IIA – Earth and Planetary Science* 325, 19–26. [https://doi.org/10.1016/S1251-8050\(97\)83268-5](https://doi.org/10.1016/S1251-8050(97)83268-5)
- Irber W. 1999: The lanthanide tetrad effect and its correlation with K/Rb, Eu/Eu*, Sr/Eu, Y/Ho, and Zr/Hf of evolving peraluminous granite suites. *Geochimica et Cosmochimica Acta* 63, 489–508. [https://doi.org/10.1016/S0016-7037\(99\)00027-7](https://doi.org/10.1016/S0016-7037(99)00027-7)
- Jackson S.E., Pearson N.J., Griffin W.L. & Belousova E.A. 2004: The application of laser ablation-inductively coupled plasma-mass spectrometry to in situ U–Pb zircon geochronology. *Chemical Geology* 211, 47–69. <https://doi.org/10.1016/j.chemgeo.2004.06.017>
- Janák M. 1994: Variscan uplift of the crystalline basement, Tatra Mts. central Western Carpathians; evidence from $^{40}\text{Ar}/^{39}\text{Ar}$ laser probe dating of biotite and P-T-t paths. *Geologica Carpathica* 45, 293–300.
- Janák M. & Onstott T.C. 1993: Pre-Alpine tectono-thermal evolution of metamorphism in the Tatra Mountains, Western Carpathians; P-T paths and $^{40}\text{Ar}/^{39}\text{Ar}$ laser probe dating. In: Seventh meeting of the European Union of Geosciences. *Terra Abstracts* 5, Suppl. 1, 238.
- Janák M., O'Brien P.J., Hurai V. & Reutl C. 1996: Metamorphic evolution and fluid composition of garnet-clinopyroxene amphibolites from the Tatra Mountains, Western Carpathians. *Lithos* 39, 57–79. [https://doi.org/10.1016/S0024-4937\(96\)00019-9](https://doi.org/10.1016/S0024-4937(96)00019-9)
- Janák M., Hurai V., Ludhova L., O'Brien P.J. & Horn E.E. 1999: Dehydration melting and devolatilization during exhumation of high-grade metapelites: the Tatra Mountains, Western Carpathians. *Journal of Metamorphic Geology* 17, 379–95.
- Janák M., Plašienka D. & Petřík I. 2001: Excursion to the Tatra Mountains, central Western Carpathians; tectonometamorphic records of Variscan and Alpine Orogeny. In: 6th meeting of the Czech Tectonics Studies Group; Donovaly, Nizke Tatry; excursion guide. *Geolines* 13, 141–148.
- Janák M., Petřík I., Konečný P., Kurylo S., Kohút M. & Madarás J. 2022: Variscan metamorphism and partial melting of sillimanite-bearing metapelites in the High Tatra Mts. constrained by Th-U-Pb dating of monazite. *Geologica Carpathica* 73, 97–122. <https://doi.org/10.31577/GeolCarp.73.2.1>
- Jurewicz E. 2005: Geodynamic evolution of the Tatra Mts. and the Pieniny Klippen Belt Western Carpathians: problems and comments. *Acta Geologica Polonica* 55, 295–338.
- Jurewicz E. 2006: Petrophysical control on the mode of shearing in the sedimentary rocks and granitoid core of the Tatra Mountains during Late Cretaceous nappe thrusting and folding, Carpathians, Poland. *Acta Geologica Polonica* 56, 159–170.
- Jurewicz E. & Baginski B. 2005: Deformation phases in the selected shear zones within the Tatra Mountains granitoid core. *Geologica Carpathica* 56, 17–28.
- Kahan Š. 1969: Eine neue Ansicht über den geologischen Aufbau des Kristallinikums der West Tatra. *Acta Geologica et Geographica Universitatis Comenianae* 18, 19–78.
- Kohút M. & Janák M. 1994: Granitoids of the Tatra Mts. Western Carpathians: field relations and petrogenetic implications. *Geologica Carpathica* 45, 301–311.
- Kohút M. & Larionov A.N. 2021: From subduction to collision: Genesis of the Variscan granitic rocks from the Tatric Superunit (Western Carpathians, Slovakia). *Geologica Carpathica* 72, 96–113.
- Kohút M. & Nabelek P. 2008: Geochemical and isotopic Sr, Nd and O: constraints on sources for Variscan granites in the Western Carpathians-implications for crustal structure and tectonics. *Journal of Geosciences* 53, 307–322.
- Kohút M. & Sherlock S.C. 2003: Laser microprobe ^{40}Ar – ^{39}Ar analysis of pseudotachylyte and host-rocks from the Tatra Mountains, Slovakia: evidence for late Palaeogene seismic/tectonic activity. *Terra Nova* 15, 417–424.
- Kohút M. & Siman P. 2011: The Goryczkova granitic type – SHRIMP dating of an original granodiorite-tonalite variety. *Mineralogia – Special Papers* 38, 113–114.
- Kohút M., Poller U., Gurk C. & Todt W. 2008: Geochemistry and U-Pb detrital zircon ages of metasedimentary rocks of the Lower Unit, Western Tatra Mountains (Slovakia). *Acta Geologica Polonica* 58, 371–384.
- Kohút M., Uher P., Putis M., Ondrejka M., Sergeev S., Larionov A. & Paderin I. 2009: SHRIMP U-Th-Pb zircon dating of the granitoid massifs in the Malé Karpaty Mountains (Western Carpathians): evidence of Meso-Hercynian successive S-to I-type granitic magmatism. *Geologica Carpathica* 60, 345–350. <https://doi.org/10.2478/v10096-009-0026-z>
- Kohút M., Hofmann M., Havrila M., Linnemann U. & Havrila J. 2018: Tracking an upper limit of the “Carnian Crisis” and/or Carnian stage in the Western Carpathians (Slovakia). *International Journal of Earth Science* 107, 321–335. <https://doi.org/10.1007/s00531-017-1491-8>
- Koppers A.A.P. 2002: ArArCALC—software for $^{40}\text{Ar}/^{39}\text{Ar}$ age calculations. *Computers & Geosciences* 28, 605–619. [https://doi.org/10.1016/S0098-3004\(01\)00095-4](https://doi.org/10.1016/S0098-3004(01)00095-4)
- Kováč M., Kral J., Marton E., Plašienka D. & Uher P. 1994: Alpine uplift history of the central western Carpathians: geochronological, paleomagnetic, sedimentary and structural data. *Geologica Carpathica* 45, 83–96.
- Kováč M., Andreyeva-Grigorovich A., Bajraktarević Z., Brzobohatý R., Filipescu S., Fodor L., Harzhauser M., Nagymarosy A., Oszczytko N., Pavelić D. & Rögl F. 2007: Badenian evolution of the Central Paratethys Sea: paleogeography, climate and eustatic sea-level changes. *Geologica Carpathica* 58, 579–606.
- Kováč M., Plašienka D., Soták J., Vojtko R., Oszczytko N., Less G., Čosović V., Fügenschuh B. & Králiková S. 2016: Paleogene palaeogeography and basin evolution of the Western Carpathians, Northern Pannonian domain and adjoining areas. *Global and Planetary Change* 140, 9–27. <https://doi.org/10.1016/j.gloplacha.2016.03.007>
- Kováč M., Márton E., Oszczytko N., Vojtko R., Hók J., Králiková S., Plašienka D., Klučiar T., Hudáčková N. & Oszczytko-Clowes M. 2017: Neogene palaeogeography and basin evolution of the Western Carpathians, Northern Pannonian domain and adjoining areas. *Global and Planetary Change* 155, 133–154. <https://doi.org/10.1016/j.gloplacha.2017.07.004>
- Kováč M., Halássová, E., Hudáčková N., Holcová K., Hyžný M., Jamrich M. & Ruman A. 2018: Towards better correlation of the Central Paratethys regional time scale with the standard geological time scale of the Miocene Epoch. *Geologica Carpathica* 69, 283–300. <https://doi.org/10.1515/geoca-2018-0017>

- Král J., Hess J.C. Kober B. & Lippolt H.J. 1997: $^{207}\text{Pb}/^{206}\text{Pb}$ and $^{40}\text{Ar}/^{39}\text{Ar}$ age data from plutonic rocks of the Strážovské vrchy Mts. basement, Western Carpathians. In: Grecula P., Hovorka D. & Putiš M. (Eds.): Geological evolution of the Western Carpathians. *Mineralia Slovaca Monograph* 253–260.
- Králíková S., Vojtko R., Sliva L., Minár J., Fügenschuh B., Kováč M. & Hók J. 2014: Cretaceous-Quaternary tectonic evolution of the Tatra Mts Western Carpathians: Constraints from structural, sedimentary, geomorphological, and fission track data. *Geologica Carpathica* 65, 307–326.
- Kroner U. & Romer R.L. 2013: Two plates — Many subduction zones: The Variscan orogeny reconsidered. *Gondwana Research* 24, 298–329. <https://doi.org/10.1016/j.gr.2013.03.001>
- Kuiper K.F., Deino A., Hilgen F.J., Krijgsman W., Renne P.R. & Wijbrans A.J. 2008: Synchronizing rock clocks of Earth history. *Science* 320, 500–504.
- La Flèche M.R., Camiré G. & Jenner G.A. 1998: Geochemistry of post-Acadian, Carboniferous continental intraplate basalts from the Maritimes Basin, Magdalen Islands, Québec, Canada. *Chemical Geology* 148, 115–136. [https://doi.org/10.1016/S0009-2541\(98\)00002-3](https://doi.org/10.1016/S0009-2541(98)00002-3)
- Leloix C., Faure M. & Feybesse J.L. 1999: Hercynian polyphase tectonics in the northeast French Massif Central: the closure of the Brévenne Devonian–Danian rift. *International Journal of Earth Sciences* 88, 409–421. <https://doi.org/10.1007/s005310050275>
- Lexa O., Schulmann K. & Ježek J. 2003: Cretaceous collision and indentation in the West Carpathians: View based on structural analysis and numerical modeling. *Tectonics* 22, 1066. <https://doi.org/10.1029/2002TC001472>
- Lister G.S. & Baldwin S.L. 1996: Modelling the effect of arbitrary P-T-t histories on argon diffusion in minerals using the Mac-Argon program for the Apple Macintosh. *Tectonophysics* 253, 83–109. [https://doi.org/10.1016/0040-1951\(95\)00059-3](https://doi.org/10.1016/0040-1951(95)00059-3)
- Lorinczi P. & Houseman G. 2010: Geodynamical models of lithospheric deformation, rotation and extension of the Pannonian Basin of Central Europe. *Tectonophysics* 492, 73–87.
- Lovera O.M., Richter F.M. & Harrison T.M. 1989: $^{40}\text{Ar}/^{39}\text{Ar}$ geothermometry for slowly cooled samples having a distribution of diffusion domain sizes. *Journal of Geophysical Research* 94, 17917–17935.
- Lovera O.M., Richter F.M. & Harrison T.M. 1991: Diffusion domains determined by ^{39}Ar release during step heating. *Journal of Geophysical Research* 96, 2057–2069.
- Ludwig K.A., 2003: Isoplot/Ex ver. 3.00, A geochronological tool kit for Microsoft Excel: Berkeley, California. *Berkeley Geochronology Center Special Publication* 4, 1–71.
- Ludwig K.R. & Mundil R. 2002: Extracting reliable U-Pb ages and errors from complex populations of zircons from Phanerozoic tuffs. *Geochimica et Cosmochimica Acta* 66, Suppl. 1, 461.
- Mahel M. 1986: Geological structure of Czechoslovak Carpathians. Part 1. Paleo-Alpine Units. *Veda*, Bratislava, 1–503 (in Slovak).
- Maluski H., Matte P. & Rajlich P. 1991: $^{40}\text{Ar}/^{39}\text{Ar}$ dating of Variscan and Alpine metamorphism in Western Carpathians. In: EUG VI, Strasbourg, 291.
- Maluski H., Rajlich P. & Matte P. 1993: $^{39}\text{Ar}-^{40}\text{Ar}$ dating of the Inner Carpathians Variscan basement and Alpine mylonitic overprinting. *Tectonophysics* 223, 313–337.
- Marko F. 1995: Dynamic analysis of fault deformation in the Central Carpathian Paleogene Basin based upon structural observations from NW and S periphery of the Levočské vrchy Mts. *MS GIÚ SAV*, Bratislava, 1–24 (in Slovak).
- Martin E., François C., Paquette J-L., Capdevila R. & Lejeune A-M. 2018: Petrogeochemistry and zircon U-Pb dating of the late Variscan Flamanville granodiorite and its Paleoproterozoic basement (Normandy, France). *Géologie de la France* 1, 34–48.
- Márton E., Tischler M., Csontos L., Fügenschuh B. & Schmid S.M. 2007: The contact zone between the ALCAPA and Tisza-Dacia mega-tectonic units of Northern Romania in the light of new paleomagnetic data. *Swiss Journal of Geosciences* 100, 109–124.
- Matte P. 1998: Continental subduction and exhumation of HP rocks in Paleozoic belts: Uralides and Variscides. Special Issue Tectonics and General History of Phanerozoic orogens. *Geological Society of Sweden G.F.F.* 120, 209–222.
- Matte P. 2001: The Variscan collage and orogeny 480–290 Ma: and the tectonic definition of the Armorica microplate: a review. *Terra Nova* 13, 122–128. <https://doi.org/10.1046/j.1365-3121.2001.00327.x>
- Mattinson J.M. 2005: Zircon U–Pb chemical abrasion (‘CA-TIMS’) method: combined annealing and multi-step partial dissolution analysis for improved precision and accuracy of zircon ages. *Chemical Geology* 220, 47–66.
- McLennan S.M. 1994: Rare earth element geochemistry and the ‘tetrad’ effect. *Geochimica et Cosmochimica Acta* 58, 2025–2033.
- Middlemost E.A.K. 1994: Naming materials in the magma/igneous rock system. *Earth-Science Reviews* 37, 215–224. [https://doi.org/10.1016/0012-8252\(94\)90029-9](https://doi.org/10.1016/0012-8252(94)90029-9)
- Moussallam Y., Schneider D.A., Janák M., Thöni M. & Holm D.K. 2012: Heterogeneous extrusion and exhumation of deep-crustal Variscan assembly: Geochronology of the Western Tatra Mountains, northern Slovakia. *Lithos* 144–145, 88–108. <https://doi.org/10.1016/j.lithos.2012.03.025>
- Moyen J-F. & Laurent O. 2018: Archaean tectonic systems: A view from igneous rocks. *Lithos* 302–303, 99–125. <https://doi.org/10.1016/j.lithos.2017.11.038>
- Moyen, J.-F., Laurent O., Chelle-Michou C., Couzinié S., Vanderhaeghe O., Zeh A., Villaros A. & Gardien V. 2017: Collision vs. subduction-related magmatism: Two contrasting ways of granite formation and implications for crustal growth. *Lithos* 277, 154–177. <https://doi.org/10.1016/j.lithos.2016.09.018>
- Mundil R., Brack P., Meie M., Rieber H. & Oberli F. 1996: High resolution U–Pb dating of Middle Triassic volcanoclastics: time-scale calibration and verification of tuning parameters for carbonate sedimentation. *Earth and Planetary Science Letters* 141, 137–151. [https://doi.org/10.1016/0012-821X\(96\)00057-X](https://doi.org/10.1016/0012-821X(96)00057-X)
- Neiva A.M.R., Williams I.S., Lima S.M. & Teixeira R.J.S. 2012: U–Pb and $^{39}\text{Ar}/^{40}\text{Ar}$ data constraining the ages of the source, emplacement and recrystallization/cooling events from late- to post-D3 Variscan granites of the Gouveia area, central Portugal. *Lithos* 153, 72–83. <https://doi.org/10.1016/j.lithos.2012.02.012>
- Nemčok J., Bezák V., Janák M., Kahan Š., Ryka W., Kohút M., Lehotský I., Wiczorek J., Zelman J., Mello J., Halouzka R., Raczkowski W. & Reichwalder P. 1993: Explanation to geological map of the Tatra Mts. 1:50,000. *GÚDŠ*, Bratislava (in Slovak).
- Nemčok M. 1993: Transition from convergence to escape: field evidence from the West Carpathians. *Tectonophysics* 217, 117–142.
- Nemčok M. & Nemčok J. 1994: Late Cretaceous deformation of the Pieniny Klippen Belt, West Carpathians. *Tectonophysics* 239, 81–109.
- Patiño Douce A.E. 1999: What do experiments tell us about relative contributions of crust and mantle to the origin of granitic magmas? *Geological Society Special Publications* 168, 55–75. <https://doi.org/10.1144/GSL.SP.1999.168.01.05>
- Pearce J.A., Harris N.B.W. & Tindle A.G. 1984: Trace element discrimination diagrams for the tectonic interpretation of granitic rocks. *Journal of Petrology* 25, 956–983. <https://doi.org/10.1093/petrology/25.4.956>

- Peterman E.M., Mattinson J.M. & Hacker B.R. 2012: Multi-step TIMS and CA-TIMS monazite U–Pb geochronology. *Chemical Geology* 312–313, 58–73. <https://doi.org/10.1016/j.chemgeo.2012.04.006>
- Petrík I., Broska I. & Uher P. 1994: Evolution of the Western Carpathian granite magmatism: Age, source rock, geotectonic setting and relation to the Variscan structure. *Geologica Carpathica* 455, 283–291.
- Pícha E.J., Stráník Z. & Krejčí O. 2006: Geology and hydrocarbon resources of the Outer western Carpathians and their foreland, Czech Republic. In: Golonka J. & Pícha F.J. (Eds.): The Carpathians and Their Foreland: Geology and Hydrocarbon Resources. *American Association of Petroleum Geologists Memoir* 84, 49–175.
- Piromallo C. & Morelli A. 1997: Imaging the Mediterranean upper mantle by P-wave travel time tomography. *Annali Di Geofisica* XL4, 963–979. <https://doi.org/10.4401/ag-3890>
- Plašienka D. 2003: Development of basement-involved fold and thrust structures exemplified by the Tatric–Fatric–Veporic nappe system of the Western Carpathians Slovakia. *Geodinamica Acta* 16, 21–38. [https://doi.org/10.1016/S0985-3111\(02\)00003-7](https://doi.org/10.1016/S0985-3111(02)00003-7)
- Plašienka D. 2018a: Continuity and episodicity in the early Alpine tectonic evolution of the Western Carpathians: How large-scale processes are expressed by the orogenic architecture and rock record data. *Tectonics* 37, 2029–2079. <https://doi.org/10.1029/2017TC004779>
- Plašienka D. 2018b: The Carpathian Klippen Belt and types of its klippen – an attempt at a genetic classification. *Mineralia Slovaca* 50, 1–24.
- Plašienka D. 2019: Linkage of the Manín and Klapce units with the Pieniny Klippen Belt and Central Western Carpathians: balancing the ambiguity. *Geologica Carpathica* 70, 35–61. <https://doi.org/10.2478/geoca-2019-0003>
- Plašienka D., Grecula P., Putiš M., Kováč M. & Hovorka D. 1997: Evolution and structure of the Western Carpathians: an overview. In: Grecula P., Hovorka D. & Putiš M. (Eds.): Western Carpathians, Evolution and structure of the Western Carpathians: an overview. *Mineralia Slovaca Corporation - Geocomplex, a.s. Bratislava*, 1–24.
- Poller U. 2000: A combination of single zircon dating by TIMS and cathodoluminescence investigations on the same grain; the CLC method-U–Pb geochronology for metamorphic rocks. In: Pagel M., Barbin V., Blanc P. & Ohnenstetter D. (Eds.): Cathodoluminescence in Geosciences. *Springer-Verlag*, Berlin, Germany, 401–414.
- Poller U. & Todt W. 2000: U–Pb single zircon data of granitoids from the High Tatra Mountains Slovakia: Implications for geodynamic evolution. *Transactions of the Royal Society of Edinburgh, Earth Science* 91, 235–243.
- Poller U., Todt W., Janák M. & Kohút M. 1999: The relationship between the Variscides and the Western Carpathians basement: New Sr, Nd and Pb–Pb isotope data from the Tatra Mountains. In: Proceedings of the International Conference CARPATHIAN GEOLOGY 2000. *Geologica Carpathica* 50, Special Issue, 131–133. <http://www.geologicacarthica.com/special-issues/50-1999/>
- Poller U., Janák M., Kohút M. & Todt W. 2000: Early Variscan magmatism in the Western Carpathians: U–Pb zircon data from granitoids and orthogneisses of the Tatra Mountains Slovakia. *International Journal of Earth Sciences* 89, 336–349.
- Poller U., Huth J., Hoppe P. & Williams I.S. 2001a: REE, U, Th, and Hf distribution in zircon from Western Carpathian Variscan granitoids: A combined cathodoluminescence and ion microprobe study. *American Journal of Science* 301, 858–867. <https://doi.org/10.2475/ajs.301.10.858>
- Poller U., Uher P., Janák M., Plašienka D. & Kohút M. 2001b: Late Cretaceous age of the Rochovce granite, Western Carpathians, constrained by U–Pb single-zircon dating in combination with cathodoluminescence imaging. *Geologica Carpathica* 52, 41–47.
- Putiš M., Ivan P., Kohút M., Spišiak J., Šiman P., Radvanec M., Uher P., Sergeev S., Larionov A., Méres S. & Demko R. 2009: Meta-igneous rocks of the West-Carpathian basement, Slovakia: indicators of Early Paleozoic extension and shortening events. *Bulletin de la Société Géologique de France* 180, 461–71.
- Rapp R.P. & Watson E.B. 1986: Monazite solubility and dissolution kinetics: implications for the thorium and light rare earth chemistry of felsic magmas. *Contributions in Mineralogy and Petrology* 94, 304–316. <https://doi.org/10.1007/BF00371439>
- Ratschbacher L., Merle O., Davy P. & Cobbold P. 1991: Lateral extrusion in the eastern Alps, Part 1: Boundary conditions and experiments scaled for gravity. *Tectonics* 10, 245–256.
- Ratschbacher L., Frisch W., Linzer H-G., Sperner B., Meschede M., Decker K., Nemčok M., Nemčok J. & Grygar R. 1993: The Pieniny Klippen Belt in the Western Carpathians of northeastern Slovakia: Structural evidence for transpression. *Tectonophysics* 226, 471–483. [https://doi.org/10.1016/0040-1951\(93\)90133-5](https://doi.org/10.1016/0040-1951(93)90133-5)
- Rauch M. 2013: The Oligocene–Miocene tectonic evolution of the northern Outer Carpathian fold-and-thrust belt: Insights from compression-and-rotation analogue modelling experiments. *Geological Magazine* 1506, 1062–1084. <https://doi.org/10.1017/S0016756813000320>
- Roca E., Bessereau G., Jawor E., Kotarba M. & Roure F. 1995: Pre-Neogene evolution of the Western Carpathians: Constraints from the Bochnia-Tatra Mountains section (Polish Western Carpathians). *Tectonics* 14, 855–873.
- Royden L.H. 1993: The tectonic expression slab pull at continental convergence boundaries. *Tectonics* 12, 303–325.
- Royden L.H. & Báldi T. 1988: Early Cenozoic tectonics and paleogeography of the Pannonian and surrounding regions. In: Royden L.H. & Horváth F. (Eds.): The Pannonian Basin. A Study in Basin Evolution. *American Association of Petroleum Geologists Memoir* 45, 1–16.
- Royden L.H. & Horváth F. 1988: The Pannonian Basin; a study in basin evolution. *American Association of Petroleum Geologists Memoir* 45, 1–394.
- Royden L.H., Horváth F. & Rumpier J. 1983: Evolution of the Pannonian basin system, 1 *Tectonics*. *Tectonics* 2, 63–90.
- Săndulescu M. 1988: Cenozoic Tectonic History of the Carpathians. In: Royden, L.H. & Horváth F. (Eds.), The Pannonian Basin; a study in basin evolution. *American Association of Petroleum Geologists Memoir* 45, 17–25.
- Schmid S.M., Pfiffner O.A., Froitzheim N., Schönborn G. & Kissling E. 1996: Geophysical geological transect and tectonic evolution of the Swiss-Italian Alps. *Tectonics* 15, 10361064.
- Schmid S.M., Pfiffner O.A., Schönborn G., Froitzheim N. & Kissling E. 1997: Integrated cross section and tectonic evolution of the Alps along the Eastern Traverse. In: Pfiffner O.A., Lehner P., Heitzmann P., Mueller St. & Steck A. (Eds.): Deep Structure of the Swiss Alps: Results of NRP 20. *Birkhauser Verlag*, Basel, Switzerland, 289–304.
- Schmid S.M., Bernoulli D., Fügenschuh B., Matenco L., Schefer S., Schuster R., Tischler M. & Ustaszewski K. 2008: The Alpine–Carpathian–Dinaridic orogenic system: correlation and evolution of tectonic units. *Swiss Journal of Geoscience* 101, 139–183.
- Schmid S.M., Fügenschuh B., Kounov A., Maţenco L., Nievergelt P., Oberhänsli R., Pleuger J., Schefer S., Schuster R., Tomljenović B., Ustaszewski K. & van Hinsbergen D.J.J. 2020: Tectonic units of the Alpine collision zone between Eastern Alps and western Turkey. *Gondwana Research* 78, 308–374. <https://doi.org/10.1016/j.gr.2019.07.005>

- Schnapperelle S., Mezger J.E., Stipp M., Hofmann M., Gärtner A. & Linnemann U. 2020: Polyphase magmatic pulses along the Northern Gondwana margin: U-Pb zircon geochronology from gneiss domes of the Pyrenees. *Gondwana Research* 81, 291–311. <https://doi.org/10.1016/j.gr.2019.11.013>
- Schuster R., Koller F., Hoeck V., Hoinkes G. & Bousquet R. 2004: Explanatory notes to the map: Metamorphic structure of the Alps metamorphic evolution of the eastern Alps. *Mitteilungen der Österreichischen Mineralogischen Gesellschaft* 149, 175–199.
- Seghedi I. & Downes H. 2011: Geochemistry and tectonic development of Cenozoic magmatism in the Carpathian–Pannonian region. *Gondwana Research* 20, 655–672. <https://doi.org/10.1016/j.gr.2011.06.009>
- Seghedi I., Downes H., Szakács A., Mason P.R.D., Thirlwall M.F., Roşu E., Pécskay Z., Márton E. & Panaiotu C. 2004: Neogene–Quaternary magmatism and geodynamics in the Carpathian–Pannonian region: a synthesis. *Lithos* 72, 117–146.
- Şengör A.M.C. 2003: The repeated rediscovery of mélanges and its implications for the possibility and the role of objective evidence in the scientific enterprise. In: Dilek Y. & Newcomb S. (Eds.): Ophiolite concept and the evolution of geological thought. *Geological Society of America Special Paper* 373, 385–445.
- Seston R., Winchester J.A., Marek A.J., Piasecki M.A., Crowley Q.G. & Floyd P.A. 2000: A structural model for the western-central Sudetes: a deformed stack of Variscan thrust sheets. *Journal of the Geological Society* 157, 1155–1167. <https://doi.org/10.1144/jgs.157.6.1155>
- Sitarz M., Gołębiewska B., Nejbart K., Dimitrova D. & Milovský R. 2021: Hydrothermal ore mineralization from the Polish part of the Tatra Mts. Central Western Carpathians. *Geology, Geophysics and Environment* 47, 159–179. <https://doi.org/10.7494/geol.2021.47.3.159>
- Sláma J., Košler J., Condon D.J., Crowley J.L., Gerdes A., Hanchar J.M., Horstwood M.S.A., Morris G.A., Nasdala L., Norberg N., Schaltegger U., Schoene N., Tubrett M.N. & Whitehouse M.J. 2008: Plešovice zircon - a new natural reference material for U-Pb and Hf isotopic microanalysis. *Chemical Geology* 249, 1–35. <https://doi.org/10.1016/j.chemgeo.2007.11.005>
- Śmigielski M., Sinclair H.D., Stuart F.M., Persano C. & Krzywiec P. 2016: Exhumation history of the Tatra Mountains, Western Carpathians, constrained by low-temperature thermochronology. *Tectonics* 35, 187–207. <https://doi.org/10.1002/2015TC003855>
- Sperner B. 1996: Computer programs for the kinematic analysis of brittle deformation structures and the Tertiary tectonic evolution of the Western Carpathians Slovakia. *Tübinger Geowiss. Arbeiten, Reihe A, Band 27*, 120.
- Sperner B., Ratschbacher L. & Nemcok M. 2002: Interplay between subduction retreat and lateral extrusion: Tectonics of the Western Carpathians. *Tectonics* 21, 1051. <https://doi.org/10.1029/2001TC901028>
- Stacey J.S. & Kramers J.D. 1975: Approximation of terrestrial lead isotope evolution by a two-stage model. *Earth and Planetary Science Letters* 26, 207–221. [https://doi.org/10.1016/0012-821X\(75\)90088-6](https://doi.org/10.1016/0012-821X(75)90088-6)
- Stampfli G.M. & Borel G.D. 2004: The TRANSMED Transects in Space and Time: Constraints on the Paleotectonic Evolution of the Mediterranean Domain. In: Cavazza W., Roure F., Spakman W., Stampfli G.M., & Ziegler P.A. (Eds.): The TRANSMED Atlas. The Mediterranean Region from Crust to Mantle. Springer, Berlin, Heidelberg. https://doi.org/10.1007/978-3-642-18919-7_3
- Stampfli G.M. & Kozur H.W. 2006: Europe from the Variscan to the Alpine cycles. *Geological Society, London, Memoirs* 32, 57–82. <https://doi.org/10.1144/GSL.MEM.2006.032.01.04>
- Starek D., Šimo V., Antolíkóvá S. & Fuksi T. 2019: Turbidite sedimentology, biostratigraphy and paleoecology: A case study from the Oligocene Zuberec Fm. (Liptov Basin, Central Western Carpathians). *Geologica Carpathica* 70, 279–297. <https://doi.org/10.2478/geoca-2019-0016>
- Steiger R.H. & Jäger E. 1977: Subcommission on geochronology: Convention on the use of decay constants in geo- and cosmochronology. *Earth and Planetary Science Letters* 36, 359–362. [https://doi.org/10.1016/0012-821X\(77\)90060-7](https://doi.org/10.1016/0012-821X(77)90060-7)
- Sun S.S. & McDonough W.F. 1989: Chemical and isotopic systematics of oceanic basalts: Implications for mantle composition and processes. *Geological Society of London Special Publications* 42, 313–345.
- Sylvester P.J. 1998: Post-collisional strongly peraluminous granites. *Lithos* 45, 29–44. [https://doi.org/10.1016/S0024-4937\(98\)00024-3](https://doi.org/10.1016/S0024-4937(98)00024-3)
- Szczygieł J. 2015: Cave development in an uplifting fold-and-thrust belt of the Tatra Mountains, Poland. *International Journal of Speleology* 44, 341–359. <https://digitalcommons.usf.edu/ijss/vol44/iss3/11>
- Szemerédi M., Lukács R., Varga A., Dunkl I., Józsa S., Tatu M., Pál-Molnár E., Szepesi J., Guillong M., Szakmány H. & Harangi S. 2020: Permian felsic volcanic rocks in the Pannonian Basin Hungary: New petrographic, geochemical, and geochronological results. *International Journal of Earth Sciences* 109, 101–125. <https://doi.org/10.1007/s00531-019-01791-x>
- Szopa K., Gawęda A., Müller A. & Sikorska M. 2013: The petrogenesis of granitoid rocks unusually rich in apatite in the Western Tatra Mts. (S-Poland, Western Carpathians). *Mineralogy and Petrology* 107, 609–627. <https://doi.org/10.1007/s00710-012-0262-2>
- Taylor S.R. & McLennan S.M. 1985: The Continental Crust: Its Composition and Evolution. Blackwell, Oxford Press, 1–312.
- Tian H., Fan M., Valencia V.A., Chamberlain K., Stern R.J. & Waite L. 2021: Mississippian southern Laurentia tuffs came from a northern Gondwana arc. *Geology* 50, 266–271. <https://doi.org/10.1130/G49502.1>
- Tichomirowa M., Gerdes A., Lapp M., Leonhardt D. & Whitehouse M. 2019a: The chemical evolution from older (323–318 Ma) towards younger highly evolved tin granites (315–314 Ma) – Sources and metal enrichment in Variscan granites of the Western Erzgebirge (Central European Variscides, Germany). *Minerals* 9, 769. <https://doi.org/10.3390/min9120769>
- Tichomirowa M., Käßner A., Sperner B., Lapp M., Leonhardt D., Linnemann U., Münker C., Ovtcharova M., Pfänder J.A., Schaltegger U., Sergeev S., von Quadt A. & Whitehouse M. 2019b: Dating multiply overprinted granites: The effect of protracted magmatism and fluid flow on dating systems (zircon U-Pb: SHRIMP/SIMS, LA-ICPMS, CA-ID-TIMS; and Rb–Sr, Ar–Ar) – Granites from the Western Erzgebirge (Bohemian Massif, Germany). *Chemical Geology* 519, 11–38. <https://doi.org/10.1016/j.chemgeo.2019.04.024>
- Tumiak K., Mazur S. & Wyszczanski R. 2000: SHRIMP zircon geochronology and geochemistry of the Orlica-Śnieżnik gneisses (Variscan belt of Central Europe) and their tectonic implications. *Geodynamica Acta* 13, 293–312. <https://doi.org/10.1080/09853111.2000.11105376>
- Uhlig V. 1903: Bau und Bild der Karpathen. In: Diener C., Hoernes R., Suess F.E. & Uhlig V. (Eds.): Bau und Bild Österreichs mit einem Vorworte von Eduard Suess. *F. Tempsky, Wien and G. Freytag, Leipzig*, 649–911 + one colored foldout map.
- van der Voo R. 2004: Paleomagnetism, oroclines, and growth of the continental crust. *GSA Today* 14, 4–9.
- van Gelder E.I., Willingshofer E., Sokoutis D. & Cloetingh S.A.P.L. 2017: The interplay between subduction and lateral extrusion: A case study for the European Eastern Alps based on analogue models. *Earth and Planetary Science Letters* 472, 82–94. <https://doi.org/10.1016/j.epsl.2017.05.012>

- Vermeesch P. 2012: On the visualisation of detrital age distributions. *Chemical Geology* 312–313, 190–194. <https://doi.org/10.1016/j.chemgeo.2012.04.021>
- Villaseñor G., Catlos E.J., Broska I., Kohút M., Hraško L., Aguilera K., Etzel T.M., Kyle J.R. & Stockli D.F. 2021: Evidence for widespread mid-Permian magmatic activity related to rifting following the Variscan orogeny Western Carpathians. *Lithos* 390–391, 106083. <https://doi.org/10.1016/j.lithos.2021.106083>
- Vozárová A., Rodionov N., Šarinová K. & Presnyakov S. 2016: New zircon ages on the Cambrian–Ordovician volcanism of the Southern Gemicum basement Western Carpathians, Slovakia: SHRIMP dating, geochemistry and provenance. *International Journal of Earth Sciences* 106, 2147–2170. <https://doi.org/10.1007/s00531-016-1420-2>
- Vozárová A., Rodionov N. & Šarinová K. 2019: Recycling of Paleoproterozoic and Neoproterozoic crust recorded in lower Paleozoic metasediments of the Northern Gemicum Western Carpathians, Slovakia: Evidence from detrital zircons. *Geologica Carpathica* 704, 298–310. <http://doi.org/10.2478/geoca-2019-0017>
- Wagreich M. 2001: A 400-km-long piggyback basin (Upper Aptian–Lower Cenomanian) in the Eastern Alps. *Terra Nova* 13, 401–406.
- Ward C.D., McArthur J.M. & Walsh J.N. 1992: Rare earth element behaviour during evolution and alteration of the Dartmoor Granite, SW England. *Journal of Petrology* 33, 785–815. <https://doi.org/10.1093/petrology/33.4.785>
- Waškowska A., Golonka J., Machowski G. & Pstrucha E. 2018: Potential source rocks in the Ropianka Formation of the Magura Nappe (Outer Carpathians, Poland)—geochemical and foraminiferal case study. *Geology, Geophysics and Environment* 44, 49–68.
- Watson E.B. & Harrison M. 1983: Zircon saturation revisited: Temperature and composition effects in a variety of crustal magma types. *Earth and Planetary Science Letters* 64, 295304.
- Weil A.B., Yonkee A. & Sussman A. 2010: Reconstructing the kinematic evolution of curved mountain belts: A paleomagnetic study of Triassic red beds from the Wyoming salient, Sevier thrust belt, U.S.A. *GSA Bulletin* 122, 3–23.
- Whalen J.B., Currie K.L. & Chappell B.W. 1987: A-type granites: Geochemical characteristics, discrimination and petrogenesis. *Contributions to Mineralogy and Petrology* 95, 407–419.
- Whitney D.L. & Evans B.W. 2010: Abbreviations for names of rock-forming minerals. *American Mineralogist* 95, 185–187.
- Wilson M. 1989: Igneous Petrogenesis. *Unwin Hyman*, London, 1–466. <https://doi.org/10.1007/978-1-4020-6788-4>
- Wolosiewicz B. 2018: The influence of the deep seated geological structures on the landscape morphology of the Dunajec River catchment area, Central Carpathians, Poland and Slovakia. *Contemporary Trends in Geoscience* 7, 21–47.
- Woodhead J.D., Hergt J.M., Davidson J.P. & Eggins S.M. 2001: Hafnium isotope evidence for ‘conservative’ element mobility during subduction zone processes. *Earth and Planetary Science Letters* 192, 331–346. [https://doi.org/10.1016/S0012-821X\(01\)00453-8](https://doi.org/10.1016/S0012-821X(01)00453-8)
- Wortel M.J.R. & Spakman W. 2000: Subduction and slab detachment in the Mediterranean-Carpathian region. *Science* 290, 1910–1917. <https://doi.org/10.1126/science.290.5498.1910>
- Zeh A., Brätz H., Millar L. & Williams I.S. 2001: A combined zircon SHRIMP and Sm–Nd isotope study of high-grade paragneisses from the Mid-German Crystalline Rise: evidence for northern Gondwanan and Grenvillian provenance. *Journal of the Geological Society* 158, 983–994. <https://doi.org/10.1144/0016-764900-186>
- Zhang Q., Wang Y., Li C.-D., Jin W.-J. & Jia X.-Q. 2006: A granite classification based on pressures. *Geological Bulletin of China* 25, 1274–1278.

Electronic supplementary material is available online:

- Supplement S1 at http://geologicacarthica.com/data/files/supplements/GC-73-6-Catlos_Supp_S1.xlsx
- Supplement S2 at http://geologicacarthica.com/data/files/supplements/GC-73-6-Catlos_Supp_S2.pdf
- Supplement S3 at http://geologicacarthica.com/data/files/supplements/GC-73-6-Catlos_Supp_S3.xlsx
- Supplement S4 at http://geologicacarthica.com/data/files/supplements/GC-73-6-Catlos_Supp_S4.xlsx
- Supplement S5 at http://geologicacarthica.com/data/files/supplements/GC-73-6-Catlos_Supp_S5.xlsx
- Supplement S6 at http://geologicacarthica.com/data/files/supplements/GC-73-6-Catlos_Supp_S6.xlsx
- Supplement S7 at http://geologicacarthica.com/data/files/supplements/GC-73-6-Catlos_Supp_S7.pdf
- Supplement S8 at http://geologicacarthica.com/data/files/supplements/GC-73-6-Catlos_Supp_S8.pdf